Title Page

Mapping transmembrane residues of Proteinase Activated Receptor 2 (PAR_2) that influence ligand-modulated calcium signaling

J Y Suen[1,#,*], M N Adams[2,#], J Lim[1], P K Madala[1], W Xu[1], A Cotterell[1], Y He[2], Mei-Kwan Yau[1], J D Hooper[2], D P Fairlie[1,*]

[1]Centre for Inflammation and Disease Research and ARC Centre of Excellence in Advanced Molecular Imaging, Institute for Molecular Bioscience, The University of Queensland, Brisbane, Qld 4072, Australia

[2]Mater Research Institute-University of Queensland, Translational Research Institute, Woolloongabba, Qld 4102, Australia.

Joint first authors

* Author for correspondence, email: d.fairlie@imb.uq.edu.au; j.suen@imb.uq.edu.au

Running Title: Ligand interactions with PAR_2

Graphical Abstract

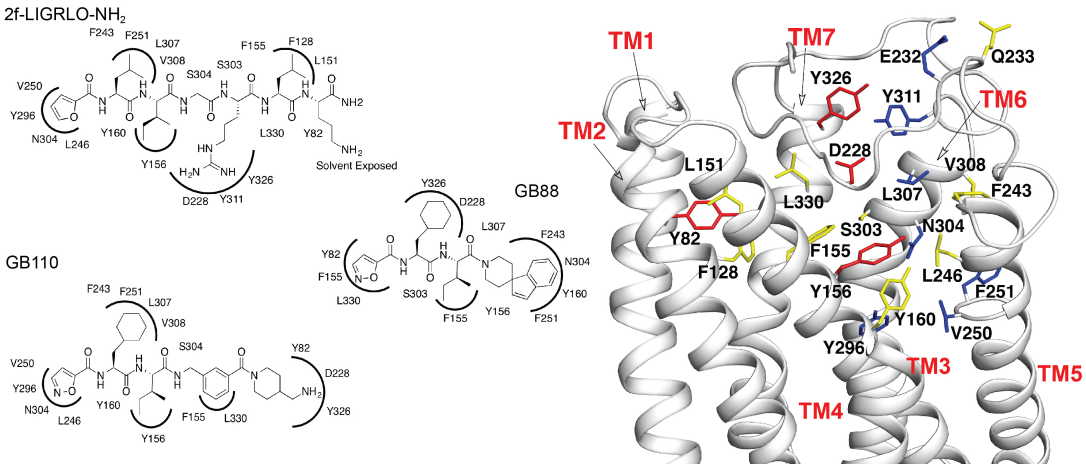

Abstract

Proteinase-activated receptor 2 (PAR_2) is a G protein-coupled receptor involved in metabolism, inflammation, and cancers. It is activated by proteolysis, which exposes a nascent N-terminal sequence that becomes a tethered agonist. Short synthetic peptides corresponding to this sequence also activate PAR_2, while small organic molecules show promising PAR_2 antagonism. Developing PAR_2 ligands into pharmaceuticals is hindered by a lack of knowledge of how synthetic ligands interact with and differentially modulate PAR_2. Guided by PAR_2 homology modeling and ligand docking based on bovine rhodopsin, followed by cross-checking with newer PAR_2 models based on ORL-1 and PAR_1, site-directed mutagenesis of PAR_2 was used to investigate the pharmacology of three agonists (two synthetic agonists and trypsin-exposed tethered ligand) and one antagonist for modulation of PAR_2 signaling. Effects of 28 PAR_2 mutations were examined for PAR_2-mediated calcium mobilization and key mutants were selected for measuring ligand binding. Nineteen of twenty-eight PAR_2 mutations reduced the potency of at least one ligand by >10-fold. Key residues mapped predominantly to a cluster in the transmembrane (TM) domain of PAR_2, differentially influence intracellular Ca^{2+} induced by synthetic agonists versus a native agonist, and highlight subtly different TM residues involved in receptor activation. This is the first evidence highlighting the importance of the PAR_2 TM region for receptor activation by synthetic PAR_2 agonists and antagonists. The trypsin-cleaved N-terminus that activates PAR_2 was unaffected by the same residues as synthetic peptides, challenging the widespread practice of substituting peptides for proteases to characterize PAR_2 physiology.

Keywords. PAR_2, protease, agonist, antagonist, mutagenesis, structure

Chemical compounds studied in this article

GB88 (PubChem CID: 73755230); GB110 (PubChem CID: 49843508); 2f-LIGRLO-NH_2 (PubChem CID: 10395438)

Abbreviations: CHO-hPAR_2, Chinese Hamster Ovary cells transfected with human PAR_2; EC_{50}, molar concentration that produces 50% of the maximum response of an agonist; ECL2, extracellular loop 2; Fluo-3, {[2-(2-{2-[Bis(carboxymethyl)amino]-5-(2,7-dichloro-6-hydroxy-3-oxo-3*H*-xanthen-9-yl)phenoxy}ethoxy)-4-methylphenyl](carboxymethyl)amino}acetic acid; GB88, 5-isoxazoyl-Cha-Ile-spiroindene-1,4- piperidine; GPCRs, G Protein-Coupled Receptors; G-protein, guanosine monophosphate protein; HBSS, Hank's Balanced Salt Solution; IC_{50}, molar concentration of an antagonist that inhibits 50% of a known concentration of agonist activity; iCa^{2+}, intracellular calcium ion; OPLS, Optimized Potentials for Liquid Simulations; PARs, Proteinase-Activated Receptors; pEC_{50}, negative logarithm of EC_{50}; SEM, standard error of the mean; pIC_{50}, negative logarithm of IC_{50}; SEM, standard error of the mean; TM, transmembrane; WT, wild type

Introduction

Proteinase-activated receptors are unique G protein-coupled receptors (GPCRs) in being self-activated following proteolytic action at their extracellular N-terminus by mainly serine proteases (Adams et al., 2011; Dery et al., 1998; Coughlin et al., 2003). This exposes a new N-terminus, the 'tethered ligand', which folds back and binds intramolecularly to induce intracellular signaling via poorly understood mechanisms (Barry et al., 2006; Ramachandran et al., 2012). Four PARs have been identified and numbered in order of their discovery (Coughlin et al., 2000).

PAR_2 is activated by serine proteases such as trypsin and tryptase but, unlike other PARs, not by thrombin (Adams et al., 2011; Barry et al., 2006; Bohm et al., 1996; Ramachandran et al., 2012). PAR_2 can also be activated by synthetic peptide agonists that mimic the N-terminal sequence of the tethered ligand (e.g. SLIGRL-NH_2 (rodent), SLIGKV-NH_2 (human), 2f-LIGRLO-NH_2 (potent derivative), P2pal-18S and 2at-LIGRL-PEG3-hdc (both lipid-tethered derivatives) (Barry et al., 2006; Hollenberg et al., 1997; Maryanoff et al., 2001; Sevigny et al., 2011; Flynn et al., 2013; Boitano et al., 2014) and by small molecule agonists (e.g. AC-55541, AC-264613 (Seitzberg et al., 2008)). Our group has identified two non-peptide ligands that were selective for PAR_2 over PAR_1 and other GPCRs, the agonist GB110 and antagonist GB88 (Barry et al., 2010; Suen et al., 2012, Suen et al., 2014). GB110 had identical agonist potency with 2f-LIGRLO-NH_2 in inducing Ca^{2+} release in multiple cell types. In addition, both GB110 and 2f-LIGRLO-NH_2, as well as proteases like trypsin and tryptase but not thrombin, were inhibited by PAR_2 antagonist GB88. In recent years PAR_2 has been implicated in many *in vitro* and *in vivo* models of inflammatory diseases as well as cancer and metabolic disorders (Adams et al., 2011; Badeanlou et al., 2011; Boitano et al., 2015; Lin et al., 2015; Ramachandran et al.,

2012; Shi et al., 2013; Vesey et al., 2013; Yau et al., 2013). The PAR_2-selective antagonist GB88 has shown beneficial effects *in vivo* in rodent models of inflammation including paw odema (Suen et al., 2012; Suen et al., 2014), collagen-induced arthritis (Lohman et al., 2012a), experimental colitis (Lohman et al., 2012b) and diet-induced obesity (Lim et al., 2013).

Ligand interactions with PAR_2 have previously been reported to involve the extracellular N-terminus and extracellular loop 2 (ECL2) (Al-Ani et al., 1999; Compton et al., 2000; Compton et al., 2002; Ma et al., 2013). A common polymorphism at position 240 potentiates PAR_2 activation by certain ligands, but not others (Compton et al., 2000; Ma et al., 2013). Also, site-directed mutagenesis indicated that by removing the glycosylation site of rat PAR2 ECL2 by mutating N222A reduced sensitivity to both trypsin and PAR_2 activating peptide (Compton et al., 2002). Mutations at positions 231-233 reportedly reduce agonist potency by ≤ 100-fold (Al-Ani et al., 1999). Each of these studies focused on the ECLs but did not examine a role for residues within the transmembrane (TM) domain of PAR_2.

As crystal structures for class A GPCRs human A2A, turkey β1 and human $P2Y_{12}$ (Warne et al., 2011; Xu et al., 2011; Zhang et al., 2014) show extensive interactions between a bound agonist and residues in TM regions, we hypothesized the TM region of PAR2 is important in influencing ligand-induced receptor activation. Based on a homology structural model of PAR_2 (Fig. 1) derived by sequence alignment with a crystallographically characterized GPCR, 28 PAR_2 mutants were constructed to investigate whether specific amino acids in the receptor affected PAR_2 activation by endogenous (trypsin induced) and synthetic agonists (2f-LIGRLO-NH_2 and GB110). 2f-LIGRLO-NH_2 was selected as the most commonly used peptide agonist for PAR2, while GB110 was selected as a potent non-peptidic

agonist and we have previously studied this agonist in detail.REF We also selected antagonist GB88 due to its reported antagonist properties both *in vitro* and *in vivo*.REF The effect of each PAR_2 mutation on ligand-induced downstream signaling was assessed to elucidate the impact of these residues on PAR_2 activation. Herein, a cluster or 'hot spot' of receptor residues that affect the activation of PAR_2 by the tested ligands has been identified. Whether other structurally diverse PAR_2 agonists or antagonists are affected by similar 'hot spot' residues remains to be determined, but this study provides valuable new insights for rational design of future PAR_2 agonists and antagonists. These prospective drugs might be used to selectively modulate PAR_2-mediated signaling and influence the pathophysiological function of PAR_2 in disease.

Methods

Sequence alignment of human PAR_2 with bovine rhodopsin crystal structure (pdb: 1U19) and Homology Modeling

The human PAR_2 sequence obtained from Swiss-Prot (accession number P55085) was aligned with the bovine rhodopsin crystal structure (pdb: 1U19, monomer) sequence using the PAM-250 matrix, which aligns the sequence based on conservation of charged, bulky aliphatic, or aromatic residues. Alignment was refined manually by examining structurally conserved regions and assessing likely TM regions using the approach of Bissantz et al (Bissantz et al., 2003). The seven TM helices were identified based on conserved residues in each putative TM helix. The alignment was used to develop coordinates for TM regions using Modeller^{TM}, with a disulfide bond constraint between C148 (TM3) and C226 (ECL2). Loop regions were developed using Modeller ^{TM} and the rhodopsin template. The model was refined to

remove steric clashes by a minor modification of the minimisation and molecular dynamics protocol above (the Newton minimisation algorithm was not performed because of the large number of atoms). In this minimisation protocol, TM backbone atoms were kept tethered to maintain TM helicity. The resulting conformation was used for ligand docking.

Homology Modeling based on nociceptin/orphanin FQ/ORL-1 receptor (pdb: 4EA3, TM sequence identity = 29%) and PAR_1 (pdb: 3VW7, TM sequence identity = 44%)

Modeller 9v10 (Sali and Blundell 1993) was used to build homology models of PAR_2 based on ORL-1 and PAR_1 crystal structures, after aligning the PAR_2 sequence with the templates using Jalview (Waterhouse et al., 2009). The models with the lowest discrete optimization protein energy (DOPE) score were further optimized for the ECL2 loop refinement in Prime (version 3.1, Schrödinger, LLC, New York, NY, 2012) using the truncated-Newton energy minimization (OPLS_2005 force field with restrained helical backbone). The final models were refined using the protein preparation wizard in Schrödinger to optimize hydrogen bond networks and for a restrained energy minimization (OPLS_2005 force field and heavy atom movement <0.5 Å).

Ligand docking

All ligands were constructed in 2D sdf format using ChemDraw. Conversion from 2D into 3D co-ordinates was performed using LigPrep in Maestro (Schrödinger). OPLS (Optimized Potentials for Liquid Simulations) force field was applied during ligand structural optimization and the protonation status of ligands was set for physiological conditions. Ligand docking was performed using GOLD (ccdc

v3.2) with default docking settings. GOLD applies a genetic algorithm during docking simulation and each ligand conformation is encoded analogously as evolution of a population of possible solutions via genetic operators to a final population. A radius of 10Å around residue F300 or F6.48 (Ballesteros Weinstein numbering scheme) (Ballesteros and Weinstein, 1995) was defined as the putative ligand-binding site. Ligands were docked in 10 independent poses (population size 100). Operator weights for mutations, migration and crossover were 95, 10 and 95 respectively. To account for partial flexibility of PAR_2, residues (F243, F155, F300, Y156, M159, L307, L330, D228, F251, L246) were defined and allowed to move according to the Chi rotamer library developed in the docking run (Lovell et al., 2000). Docked poses were ranked using the internal Gold score (Jones et al., 1997) and manual inspection of interactions with receptor. Final analysis and visualisation of protein-ligand interactions were performed using Pymol. To cross-check the results from the Rhodopsin-derived PAR_2 model, the ligands were also subsequently docked into PAR2 homology models built from ORL-1 and PAR_1 crystal structures. The PAR_2 homology structures and ligand docking protocols using these models are detailed elsewhere (Perry et al, 2015).

Cell culture and reagents

Cell culture reagents were purchased from Invitrogen (Carlsbad, CA) and Sigma Aldrich (St. Louis, MO). Flp-In Chinese Hamster Ovary (CHO)-K1 cells (Invitrogen) were maintained in Ham's F12 media containing 10% FBS and 2 mM L-glutamine in 5% CO_2 at 37 ^{o}C. PAR_2 peptide agonist (2f-LIGRLO-NH_2), non-peptide agonist (GB110) and non-peptide antagonist (GB88) were synthesized in-house (Barry et al., 2010). A23187 was purchased from Sigma-Aldrich, Fluo-3 AM and Pluronic F127

195 from Sapphire Bioscience (NSW, Australia), and assay plates from Corning (New
196 York, NY).
197
198 *Vector construction and transfection*
199 cDNA encoding human PAR_2 with a C-terminal FLAG epitope (DYKDDDDK)
200 was subcloned into a pcDNA5/FRT vector (Life technologies/invitrogen) using a
201 BamHI restriction enzyme site. Site directed mutagenesis was performed using a
202 QuickChange kit (Stratagene) according to manufacturer's instructions to generate
203 individual receptor mutants (Table 1). Primer sequences are available upon request.
204 All constructs were sequenced at the Australian Genomic Research Facility (St Lucia,
205 Australia). Stably expressing cells were generated following manufacturer's
206 instructions. PAR_2-pcDNA5/FRT constructs were cotransfected with Flp-recombinase
207 expression vector pOG44 (1:9 pcDNA5/FRT:pOG44) into Flp-In CHO-K1 cells using
208 Lipofectamine 2000. Stable polyclonal populations of transfected cells were selected
209 in media containing 600 μg/mL hygromycin B.
210
211 *Crude membrane preparation and Western blot analysis*
212 Expression of wildtype and each PAR_2 mutant was assessed as described (Adams
213 et al., 2011; Adams et al., 2012). Crude membrane preparations were collected by
214 isotonic cell shock and mechanical disruption followed by ultracentrifugation
215 (100,000 g for 60 min at 4 °C) to pellet the membrane fraction. Fractions were
216 resuspended in lysis buffer (50 mM Tris pH 7.4, 150 mM NaCl, 5 mM EDTA, 1%
217 Triton X-100 (v/v) and 1× protease inhibitor cocktail (Roche)) before quantification
218 using a BCA assay kit from Pierce (Thermo Fisher Scientific, Scoresby, Australia).
219 Equal amounts of membrane fractions were separated by SDS-PAGE and transferred

to nitrocellulose membrane. Membranes blocked in Odyssey blocking solution from LiCor (Millennium Science, Surrey Hills, Australia) were incubated with goat anti-PAR_2 N19 (Santa Cruz) and mouse anti-Pan Cadherin (Millipore) antibodies overnight at 4 °C. Membranes were washed and incubated with species appropriate IRdye 700 or 800 secondary antibodies at ambient temperature for 45 min before washing to minimize non-specific signals followed by scanning on an Odyssey infrared imaging system (LiCor).

Flow cytometry analysis

Cell surface expression of wildtype and each PAR_2 mutant was assessed as described (Adams et al., 2012). Cells (2.5×10^5) dissociated non-enzymatically from cell culture flasks were washed and stained with goat anti-PAR_2 N19 antibody (2 µg / 1×10^6 cells) in buffer (2% BSA in PBS) for 30 min at 4°C. Cells were washed and stained with AlexaFluor 488-conjugated donkey anti-goat secondary antibody before analysis on a Beckman Coulter FC500 flow cytometer. Events were counted (20,000) and mean fluorescence intensity (MFI) was used to assess cell surface PAR_2 after subtracting MFI values from cells incubated only with secondary antibody. Competitive ligand binding and calcium mobilization assays are well established methods reported in Supporting Material.

Competitive binding assay

Assays were performed as described (Hoffman et al., 2012). Cells were seeded overnight in a 384-well plate at a density of 24000 cells per well. On the day of experiment, media was aspirated and cells were washed with PBS followed by 2% BSA blocking for 1h at 37°C. After blocking, cells were simultaneously exposed to

concentrations of 2f-LIGRLO(dtpa)-NH_2 and 2f-LIGRLO-NH_2 (100 μM) for 15 min. Cells were washed thrice with PBS supplemented with 20 μM EDTA, 0.01% Tween and 0.2% BSA. After washings, cells were incubated with 40 μl of DELFIA enhancement solution (Perkin Elmer) for 90 min. Fluorescence was determined with TRF analysis (Pherastar FS, BMG Labtech): 340 nm excitation followed by 400 μs delay before a 400 μs 615 nm emission.

Intracellular calcium mobilization

Cells were grown to 80% confluence. Prior to experiment, cells were seeded overnight in 96-well black wall, clear bottom, plates at ~5 x 10^4 cells per well. On the day of the experiment, supernatant was removed and cells were incubated in dye loading buffer (Hank's Balanced Salt Solution (HBSS) with 4 μM Fluo-3, 0.04% pluronic acid, 1% fetal bovine serum (FBS) and 2.5 mM probenecid) for 1 h at 37 °C. Cells were washed twice with HBSS and transferred to a FLIPR Tetra plate reader (Molecular Device, Sunnyvale CA) for agonist injection and fluorescence measurements. PAR_2 agonists were added 10 s after reading commenced at various concentrations and fluorescence was measured in real time using excitation 480 nm and emission 520 nm. HBSS was prepared in-house, all other reagents were from Invitrogen (Carlsbad), plates from Corning. Calcimycin (A23187, Sigma Aldrich) was used to measure maximum fluorescence, with individual results normalized accordingly.

Statistical analysis

Data were analyzed in GraphPad Prism (GraphPad Software, San Diego, CA) using ANOVA or Student's t-test with values as mean ± SEM ($n \geq 3$). Data are

presented as the mean of the entire data set. Significance was determined by $P<0.05$. When plotted in concentration-response curve, intracellular Ca^{2+} response was normalized against highest concentration of respective agonist in CHO-$hPAR_2$WT. Concentration-response curves were fitted in GraphPad Prism with a standard Hill slope of 1 (three-parameter fit).

Results

Homology Structural Models of PAR_2

A PAR_2 structural homology model was generated by sequence alignment of human PAR_2 to the crystal structure of bovine rhodopsin (pdb: 1U19; Palczewski et al., 2000), at a time when this was the only reported GPCR crystal structure. The PAR_2 homology model was submitted to SwissModel portal (http://swissmodel.expasy.org/) for quality and stereochemical properties check. The assessment of model quality-related parameters (such as Qmean6 score, dfire energy and Ramachandran statistics) were compared with the original crystal structure of the bovine rhodopsin (1U19). The PAR_2 homology model gave a RMSD value of 0.37 compared to the bovine rhodopsin. Qmean6 score (PAR_2 0.41, Rhodopsin 0.40) is a linear combination of six structural descriptors and a higher Qmean6 (range between 0 and 1) reflects strong reliability of the model. DFire (PAR_2 -465.5; Rhodopsin -557.8) is an all-atom statistical potential term used to assess non-bonded atomic interactions in the protein model. The homology model of PAR_2 produced comparable scores for these two components, relative to the template from which they were constructed. Furthermore, all residues in the rhodopsin based homology model were located in the favored and allowed ϕ-ψ regions from the Ramachandran plot analysis, suggesting that the constructed homology model was both energetically and stereochemically reliable.

In silico docking of three ligands in a PAR_2 homology structural model

Interactions between PAR_2 and three synthetic ligands were examined *in silico* (Fig. 1A). Synthetic ligands used *in silico* were the two PAR_2 agonists, 2f-LIGRLO-NH_2 (Kanke et al., 2005; McGuire et al., 2004) and GB110 (Barry et al., 2010), as

well as the PAR_2 antagonist GB88 (Suen et al., 2012) (Fig. 1B-D). All three ligands were also experimentally assessed in an intracellular calcium mobilization assay.

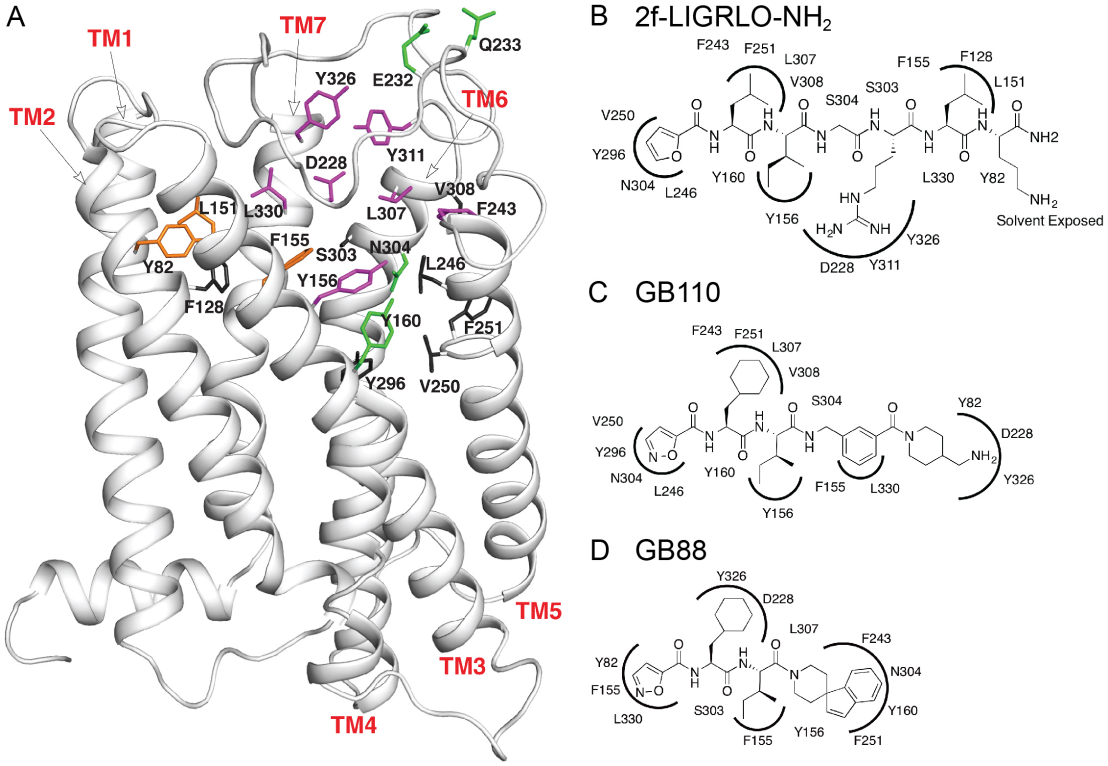

FIGURE 1. Putative ligand-receptor interactions. (A) 2f-LIGRLO-NH_2, GB110, and GB88 were each docked into a homology structural model of PAR_2 generated from the crystal structure of bovine rhodopsin. The docking result was then cross-checked by docking into PAR2 models generated from ORL-1 and PAR_1. Residues are colored according to their importance in the three models (magenta, RHO/ORL-1/PAR1), two models (orange, RHO/ORL-1; green, RHO/PAR_1) or the RHO model only (black). (B-D) Residues predicted to mediate PAR_2 interaction with (B) 2f-LIGRLO-NH_2, (C) GB110, and (D) GB88.

Modeling predicted that both agonists would occupy a similar binding region within the TM domain of PAR_2. 2f-LIGRL-NH_2 rather than 2f-LIGRLO-NH_2 was

317 docked since the ornithine does not contribute significantly to agonist potency and
318 can confound docking orientations due to its charged sidechain finding alternative
319 binding sites on its own (Kanke et al., 2005; McGuire et al., 2004). The similar
320 components of 2f-LIGRLO-NH_2 and GB110 (2-furoyl vs isoxazole, Leu vs Cha, Ile
321 vs Ile) were predicted to dock into pockets formed by TM3 (Y156, Y160), TM5
322 (F243, L246, V250) and TM6 (N304, L307, V308) (Fig. 1B,C). The other ligand
323 components were predicted to orient slightly differently for the two agonists. R4 in
324 2f-LIGRLO-NH_2 was predicted to orient towards residues at the top of TM6 (Y311)
325 and TM7 (Y326) as well as ECL2 (D228) (Fig. 1B). However, the terminal
326 aminomethyl piperidine group of GB110 was predicted to project between TM2
327 (Y82) and TM7 (L330) (Fig. 1C). The antagonist GB88 docked in a similar binding
328 site, but its orientation was reversed with the isoxazole in a small pocket formed by
329 Y82, F155 and L330 (Fig. 1D). Its cyclohexylalanine oriented into space between
330 TM6 (Y307) and TM7 (Y326), while isoleucine oriented towards F155. The bulky
331 spiroindenepiperidine occupied a hydrophobic site surrounded by Y156, Y160, F243,
332 F251 and N304 (Fig. 1D). These predicted sites suggested a cluster of amino acids
333 within the TM region of PAR_2 that might be expected to influence ligand potencies
334 and efficacies.

335 Following completion of this study, crystal structures of human
336 nociceptin/orphan FQ receptor (4EA3) (Thompson et al., 2012) and the antagonist
337 bound PAR_1 receptor (3VW7) (Zhang et al., 2012) provided alternative templates for
338 also constructing homology models of PAR_2. When the above ligands were docked
339 into either of these new models of PAR_2 based on the different template crystal
340 structures, the key residues inferred from the rhodopsin-based model of PAR_2 (Y82,
341 L151, F155, Y156, F243, L307, Y311, Y326, L330) were also found in the ORL-1

342 derived model of PAR_2, while Y156, Y160, E232, F243, L307, Y311, Y326, L330
343 were also found in the PAR_1-based model of PAR_2. In particular, both models
344 predicted 2f-LIGRLO-NH_2 to make several polar interactions with residues Y311,
345 $D228^{ECL2}$, whereas Y156 from the ORL-1 model was also predicted to form polar
346 contact with the ligand. The rest of the residues were mainly predicted to contribute to
347 hydrophobic and aromatic interactions. The major difference seen was the position of
348 the 2f group, which was docked within a pocket between TM2 and TM7 in the ORL-1
349 based model, while in the PAR1 based model this group was docked between TM5
350 and TM6 (Perry et al., 2015). Of the residues shown ahead to cause >30-fold
351 reduction in receptor activation, only Y296 and N304 were not predicted from the
352 new homology models of PAR_2. Interestingly, those two residues are the deepest in
353 the TM 7-helix bundle and might be indirectly impacted through knock-on or
354 conformational changes during receptor activation. The new models of PAR_2 thus
355 supported the above predictions based on the bovine rhodopsin derived PAR_2
356 homology structure, while presenting some new clues for further refinement of the
357 PAR_2 model.

358 Based on these predicted ligand-binding sites, 18 PAR_2 TM residues (Y82, F128,
359 L151, F155, Y156, Y160, F243, L246, V250, F251, Y296, S303, N304, L307, Y308,
360 Y311, Y326, L330) and an ECL2 residue (D228) were chosen for mutagenesis to
361 investigate the experimental effect of these mutations on ligand-induced downstream
362 signaling. Two additional ECL2 residues, E232 and Q233, were also selected for
363 mutation on the basis of previous studies (Al-Ani et al., 1999), giving a total of 21
364 amino acids to be mutated. Fig. 1 displays these residues revealing where they cluster
365 within or near the TM region of PAR_2, thereby forming putative 'hot spots' in PAR_2
366 that might dictate agonist and antagonist ligand activity.

Mutation of PAR_2 in stably expressing cell lines

Site directed mutagenesis generated expression constructs encoding the relevant amino acid mutated to alanine (Y82, L151, D228, E232, Q233, F243, L246, V250, F251, Y296, S303, L307, Y308), chosen to inform the importance of larger sidechains for space-filling; to leucine (Y160) or tryptophan (L330), to test the importance of aromaticity; or with 6 residues mutated to both small alanine and bulkier hydrophobic leucine (F128, F155, Y156, N304, Y311, Y326). A construct encoding the double mutant E322A/Q233A was also generated to allow comparison with a previous study on rat PAR_2 (Al-Ani et al., 1999) to give a total of 28 PAR_2 mutant expression constructs. To examine the impact of these mutations on ligand-induced signaling, CHO-K1 cells were generated that stably expressed each of the 28 mutants or wildtype PAR_2. The impact of each mutation on structural integrity of PAR_2 and its cell surface expression was assessed using Western blot and flow cytometry. Western blot analysis revealed that each PAR_2 was expressed at consistent levels as a characteristic ladder of bands from ~30-80 kDa (Fig. 2A, upper panel), as described (Adams et al., 2012). Similarly, flow cytometry demonstrated that cell surface expression was comparable for wildtype and each mutant PAR_2 (Fig. 2A, lower panel). These data indicated structurally integrity and PAR_2 surface expression on CHO-K1 cells. Importantly, cells transfected with vector failed to produce any significant signal in response to synthetic agonists 2f-LIGRLO-NH_2 and GB110 or tethered ligand formed by trypsin cleavage, in contrast with cells transfected with wildtype PAR_2 (Fig. 2B-D). This indicates that calcium mobilization in transfected cells was PAR_2 mediated.

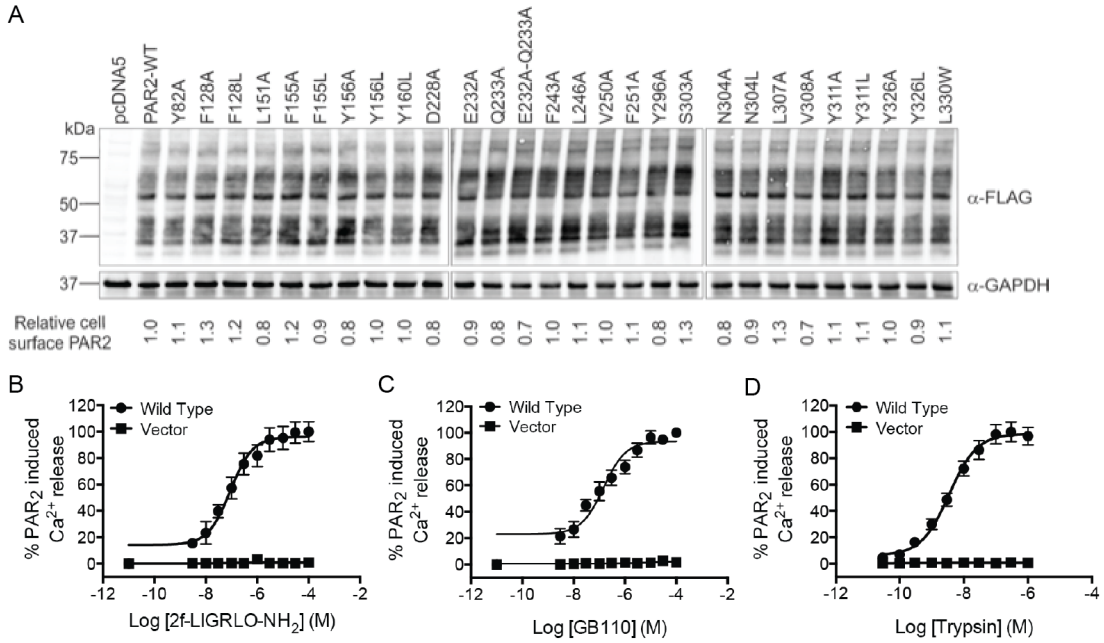

FIGURE 2. PAR_2 expression and activation. (A) Expression and cell surface levels of wild type and mutant PAR_2 in CHO-K1 cells. *Upper:* Western blot analysis, performed on equal amounts of crude membrane preparations using an anti-Flag antibody, shows that PAR_2 wildtype and mutants were expressed at similar levels. *Lower:* Flow cytometry analysis on non-permeabilized cells using anti-PAR_2 N19 antibody confirmed that wildtype and PAR_2 mutants were expressed at the cell surface. Levels ranged within +/- 10% of the wildtype receptor for 15 of the mutants with another 8 within +/- 20%. Cell surface levels of PAR_2-F128A, E232A-Q233A, S303A, L307A and V308A were within +/- 30% of wildtype PAR_2. (B-D): Intracellular Ca^{2+} mobilization by PAR_2 agonists in CHO-PAR_2 wild type vs CHO-hPAR_2 empty vector. All three agonists (B, 2f-LIGRLO-NH_2; C, GB110; D, Trypsin) stimulated intracellular calcium release in CHO cells transfected with wild type PAR_2 (circle) but failed to induced any response in CHO cells transfected with empty vector (square). Data points = means of 3 experiments in triplicates (n=3), bars = S.E.

409 *Effect of PAR_2 mutations on synthetic agonist potencies*

410 The real impact of PAR_2 mutations on signaling was experimentally assessed by
411 intracellular calcium release induced by escalating doses of 2f-LIGRLO-NH_2 and
412 GB110. The pEC_{50} and fold changes relative to wildtype PAR_2 are shown in Table 1.
413 Four mutations induced enormous reductions (>100 fold) in ligand potencies, three
414 located in the TM domain (Y82A, Y156A, Y326A) and the fourth in ECL2 (D228A)
415 (Table 1). All four mutations had similar effects on potency of both agonists 2f-
416 LIGRLO-NH_2 and GB110 (Fig. 3A-D). Six other TM mutations (Y156L, F251A,
417 Y296A, N304A, N304L, Y311A) along with ECL2 mutation E232A also induced
418 substantial (>10 fold) reductions in signaling by both agonists (Table 1). Overall, 19
419 of 28 mutant PAR_2 cell lines revealed ≥10 fold attenuation in activity for at least one
420 agonist (Fig. 3E). When analyzed by scatter plot, there was a high correlation between
421 mutation-induced fold changes in activity of 2f-LIGRLO-NH_2 versus GB110 (Fig.
422 3F), indicating that these ligands were affected by a similar set of residues of PAR_2.

Table 1 Effect of PAR_2 mutations on potencies of agonists inducing Ca^{2+} release in PAR_2 expressing CHO-K1 cells

	2f-LIGRLO-NH_2 (n=4)		GB110 (n=4)		Trypsin (n=4)	
PAR_2 Mutation	pEC_{50}	Fold	pEC_{50}	Fold	pEC_{50}	Fold
Wild Type	7.4 ± 0.2		7.5 ± 0.1		8.7 ± 0.1	
Vector	inactive		inactive		inactive	
Y82A	< 4	>2000	< 4	>2000	7.6 ± 0.4	13
F128A	6.8 ± 0.2	4	6.7 ± 0.3	6	8.1 ± 0.2	4
F128L	6.4 ± 0.1	11	6.5 ± 0.2	9	8.5 ± 0.2	1
L151A	7.3 ± 0.2	1	7.2 ± 0.5	2	8.3 ± 0.1	3
F155A	7.0 ± 0.3	3	6.5 ± 0.2	10	8.2 ± 0.2	3
F155L	6.3 ± 0.1	12	6.7 ± 0.1	6	8.3 ± 0.3	2
Y156A	5.3 ± 0.2	110	5.1 ± 0.2	250	7.9 ± 0.1	6
Y156L	6.2 ± 0.1	16	5.7 ± 0.2	59	8.0 ± 0.1	5
Y160L	6.6 ± 0.2	6	6.6 ± 0.2	7	7.8 ± 0.1	8
D228A	5.3 ± 0.2	140	5.3 ± 0.2	170	7.8 ± 0.2	7
E232A	6.1 ± 0.4	18	6.1 ± 0.3	28	7.9 ± 0.1	7

Q233A	7.2 ± 0.1	2	8.5 ± 0.2	0.1	8.2 ± 0.1	3
E232AQ233A	6.6 ± 0.1	6	8.2 ± 0.1	0.2	8.5 ± 0.1	2
F243A	6.4 ± 0.2	11	6.7 ± 0.2	7	8.5 ± 0.2	2
L246A	6.3 ± 0.2	13	6.5 ± 0.1	9	8.0 ± 0.2	4
V250A	7.2 ± 0.3	2	6.3 ± 0.4	17	8.3 ± 0.2	2
F251A	5.9 ± 0.1	28	6.2 ± 0.1	18	8.0 ± 0.2	5
Y296A	5.7 ± 0.2	51	6.0 ± 0.2	30	7.5 ± 0.1	17
S303A	6.7 ± 0.3	5	6.6 ± 0.2	7	8.4 ± 0.2	2
N304A	5.9 ± 0.1	29	6.1 ± 0.2	27	7.6 ± 0.2	12
N304L	5.8 ± 0.1	40	5.8 ± 0.1	50	7.1 ± 0.1	37
L307A	6.8 ± 0.2	4	5.8 ± 0.1	54	8.4 ± 0.2	2
V308A	7.2 ± 0.3	2	7.4 ± 0.2	1	8.4 ± 0.2	2
Y311A	5.6 ± 0.1	62	5.8 ± 0.1	44	8.2 ± 0.1	3
Y311L	7.0 ± 0.2	2	7.3 ± 0.3	2	8.0 ± 0.1	5
Y326A	5.0 ± 0.2	240	5.3 ± 0.1	160	7.8 ± 0.2	7
Y326L	6.7 ± 0.2	6	6.2 ± 0.1	19	7.9 ± 0.1	5
L330W	7.2 ± 0.3	2	7.3 ± 0.3	1	8.2 ± 0.2	3

n = number of independent experiments

$pEC_{50} = -\log(EC_{50})$

pEC_{50} ± S.D., Fold Change = EC_{50} Mutant/EC_{50} Wild Type

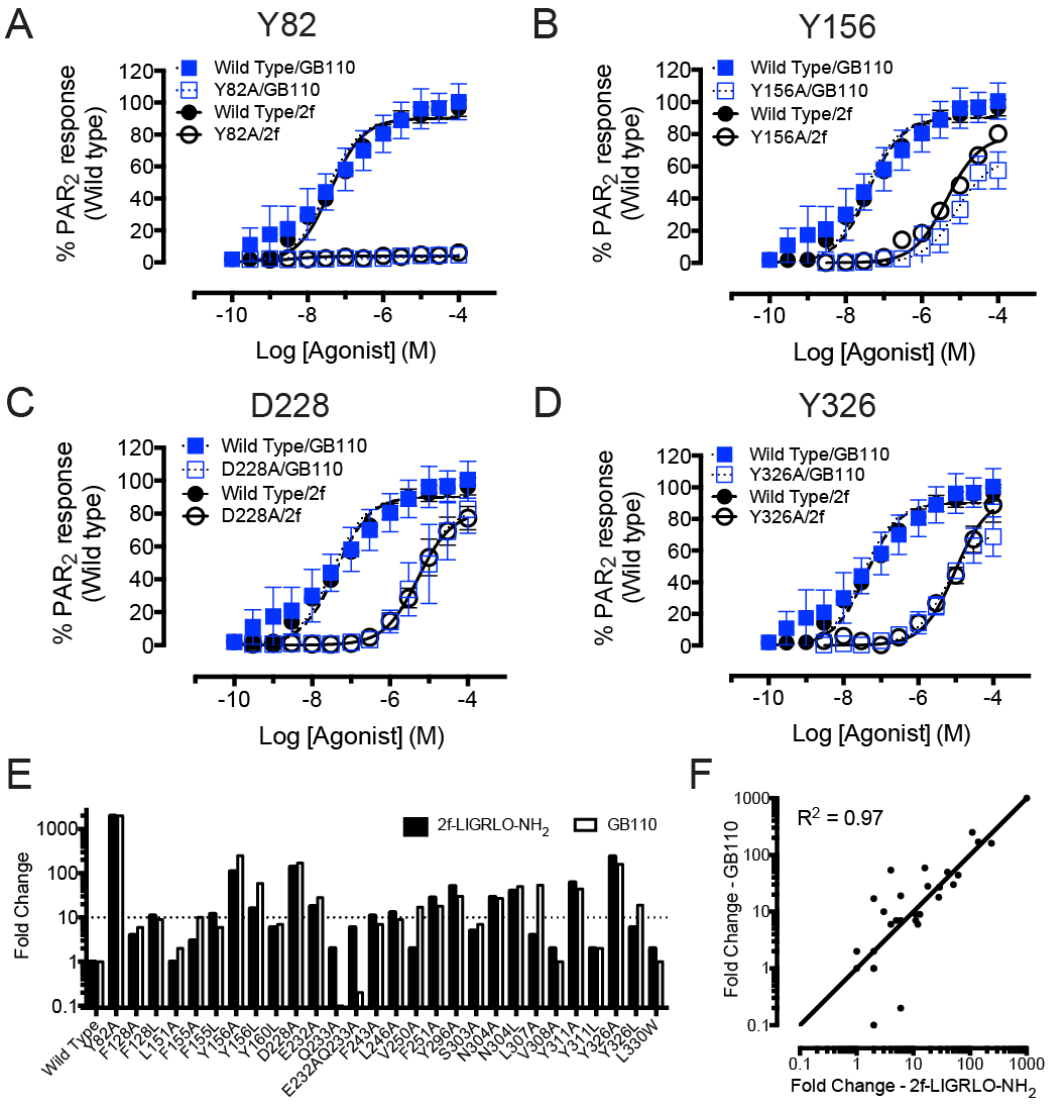

423

424 **FIGURE 3.** Concentration response curves of 2f-LIGRLO-NH_2 and GB110 on
425 various PAR_2 mutants. Intracellular calcium release induced by PAR_2 activation was
426 plotted against various concentrations of 2f-LIGRLO-NH_2 (black) and GB110 (blue).
427 (A-D) Mutations (A, Y82A; B, Y156A; C, D228; D, Y326A) have similar effects on
428 both PAR2 agonists. Data points = means of 3 experiments in triplicates (n=3), bars =
429 S.E. (E,F) Summary of influences of PAR_2 residues on synthetic agonist potencies of
430 2f-LIGRLO-NH_2 vs GB110. (E) Effect of mutation on agonist potencies. Fold
431 changes calculated by EC_{50} of PAR_2 mutant over EC_{50} of PAR_2 wild type (WT). (F)
432 Correlation study of effects of mutation on agonist potencies. $R^2 = 0.97$.

433

CHO cells expressed with wild type or vectors only or 8 mutated PAR_2 were selected for measuring agonist affinity. Y156A, D228A and Y326A were chosen due to their significant impact on PAR_2-induced calcium release (Table 1). Five neighboring mutants (F155A, Y156L, Y160L, Y326L, L330W) were also selected. A receptor saturation assay was used to calculate K_d for 2f-LIGRLO(dtpa)-NH_2 on each cell line (Fig. 4). Control experiments with PAR_2 WT gave K_d 0.67 μM and the tagged peptide failed to bind to CHO cells not expressing PAR_2. This suggested specific binding to human PAR_2. Similar to the negative control, Y156A, D228A and Y326A all failed to give any measurable saturation, indicating that labeled peptide was not able to selectively bind to the mutated receptor expressed. In contrast, each of the remaining 5 mutants was able to produce a K_d ~3-5 fold weaker than wild type.

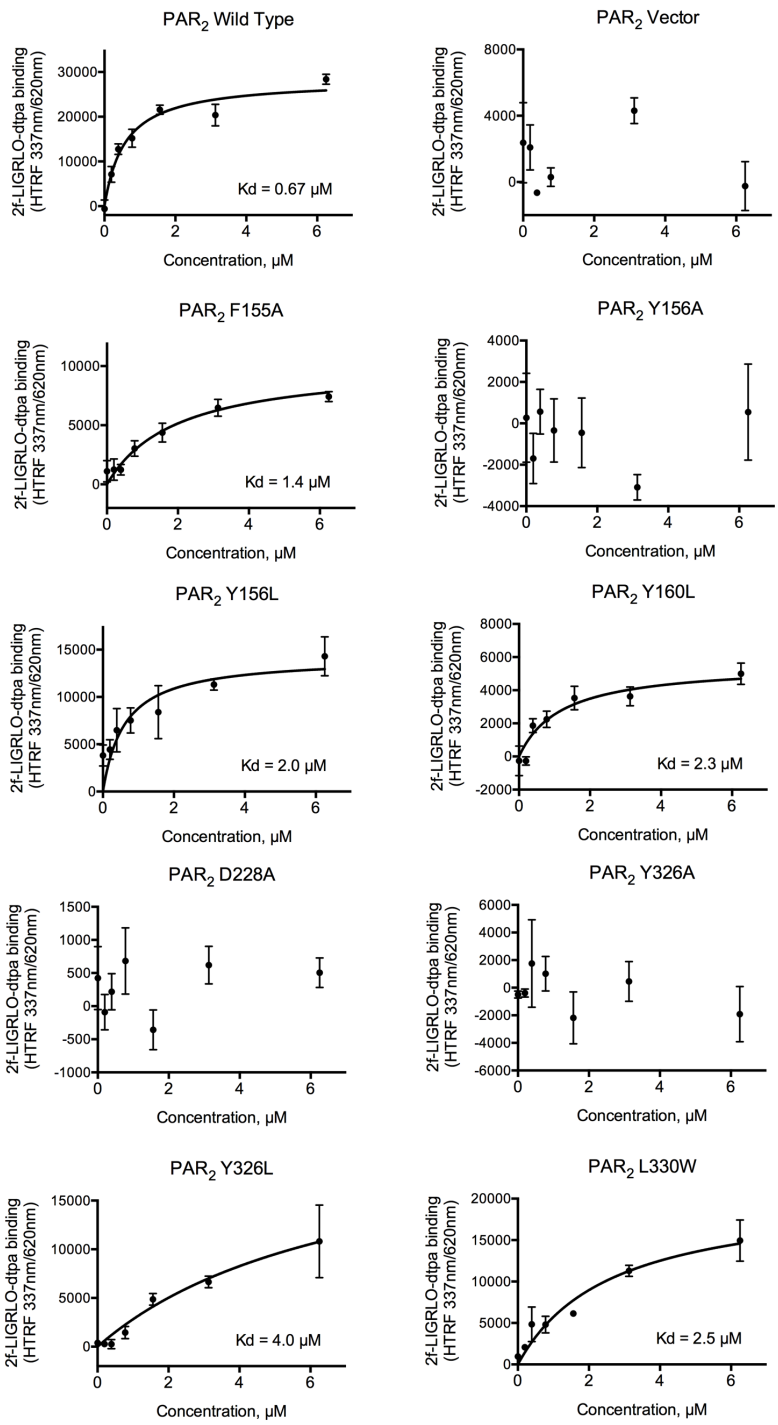

446

447 **FIGURE 4.** Representative saturation curves for 2f-LIGRLO(dtpa)-NH_2 specific
448 binding to wild-type and mutant PAR_2 receptors. Specific binding was measured by
449 incubating CHO cells expressed with various PAR_2 mutants with different
450 concentrations of 2f-LIGRLO(dtpa)-NH_2 and 2f-LIGRLO-NH_2 (100 µM). K_d was
451 calculated from 3 or more independent experiments.

452

453 *Effects of PAR_2 mutations on trypsin potency*

454 The agonist potency was measured for trypsin on the same 28 mutated PAR_2
455 transfected CHO cell lines in Table 1. Only four mutations (Y82A, Y296A, N304A,
456 N304L) caused > 10-fold reductions in agonist potencies (Fig. 5A-C) and all were in
457 the TM region of PAR_2, indicating the importance of the TM region in protease-
458 mediated PAR_2 activation. However, in contrast to the two synthetic agonists, most
459 mutations examined induced < 10-fold reductions in trypsin-induced agonist potency
460 (Fig. 5D). This suggested that the tethered ligand was not as susceptible to the same
461 mutations as the two synthetic agonists. In support of this conclusion, there was no
462 significant correlation between effects of mutants on calcium mobilization induced by
463 trypsin vs by each synthetic agonist (Fig. 5E,F).

464

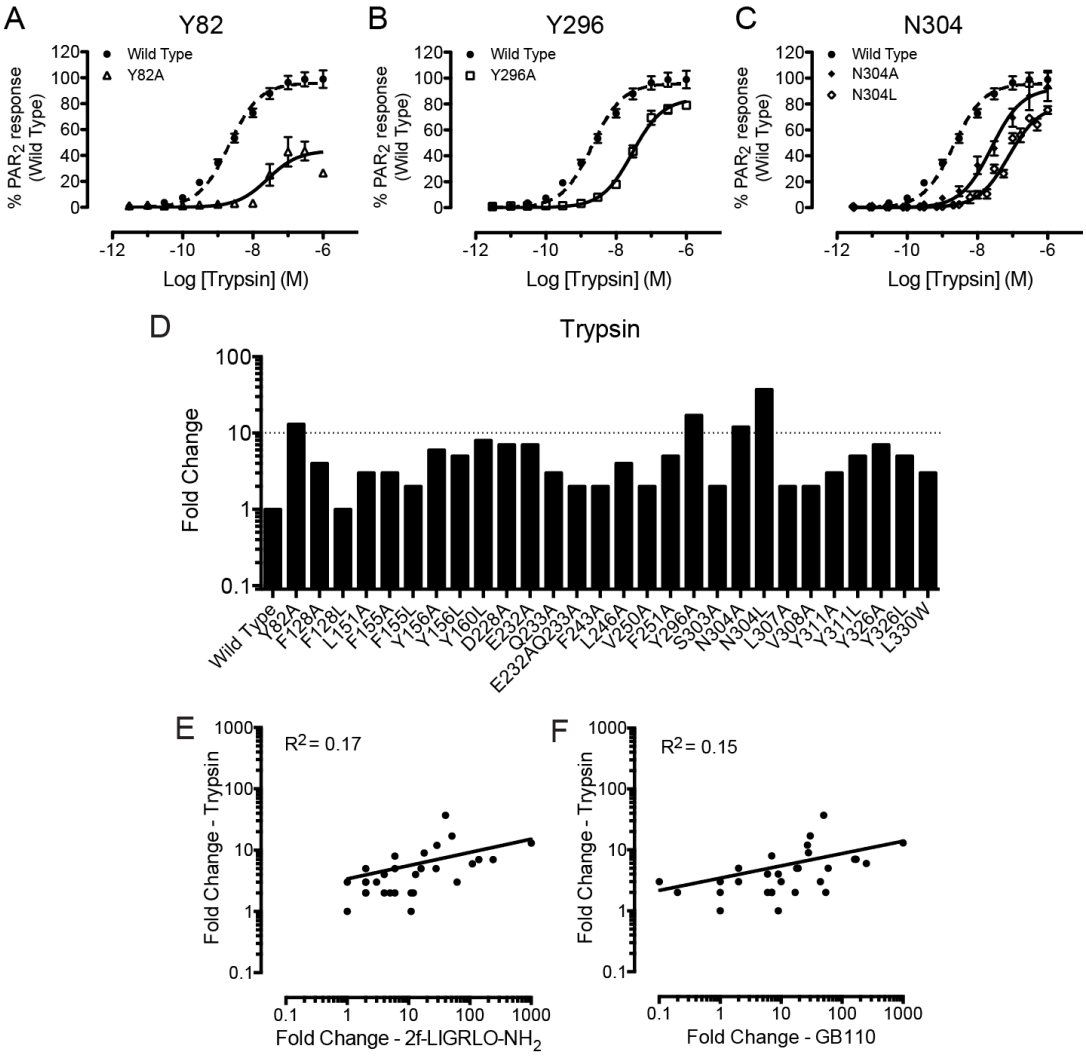

FIGURE 5. Summary of influences of PAR_2 residues on serine protease trypsin. (A-C) Concentration response curves of trypsin on various PAR_2 mutants. Intracellular calcium release induced by PAR_2 activation was plotted against various concentrations of trypsin. Mutations (A, Y82A; B, Y296A; C, N304A, N304L) all lowered potencies of trypsin by >10 fold. Data points = means of 3 experiments in triplicates (n=3), bars = S.E. (D) Effects of mutation on trypsin potencies. Fold changes calculated by EC_{50} of PAR_2 mutant over EC_{50} of PAR_2 wild type (WT). (E-F) Correlation studies of effects of mutations on trypsin against (E) 2f-LIGRLO-NH_2 or (F) GB110.

Effects of PAR_2 mutation on antagonist potency

GB88 is a small molecule reported to effectively antagonize calcium release in human cells by all PAR_2 agonists, including the peptides SLIGRL-NH_2, SLIGKV-NH_2, 2f-LIGRLO-NH_2, the peptidomimetic GB110, and proteases like trypsin, tryptase and cathepsin S (Barry et al., 2010; Suen et al., 2012; Zhao et al., 2014a). In order to determine the impact of mutation of PAR_2 residues on GB88 potency, cells were first incubated with escalating doses of GB88 and stimulated with trypsin at EC_{80} determined from Table 1. The pIC_{50} and fold change (mutant versus wildtype PAR_2) values are listed in Table 2. GB88 could not be tested against CHO-hPAR_2Y82A cells, as the agonist response generated by trypsin was too small to produce a significant signal-to-noise ratio. Overall, seven mutants derived from changes at 5 positions (Y156, D228, N304, L307, Y326) on PAR_2 were found to inactivate GB88 (<40% max inhibition) antagonism of trypsin-induced intracellular calcium release (Fig. 6). In addition, L151A and F243A mutations reduced potency of GB88 by greater than 10-fold (Table 2).

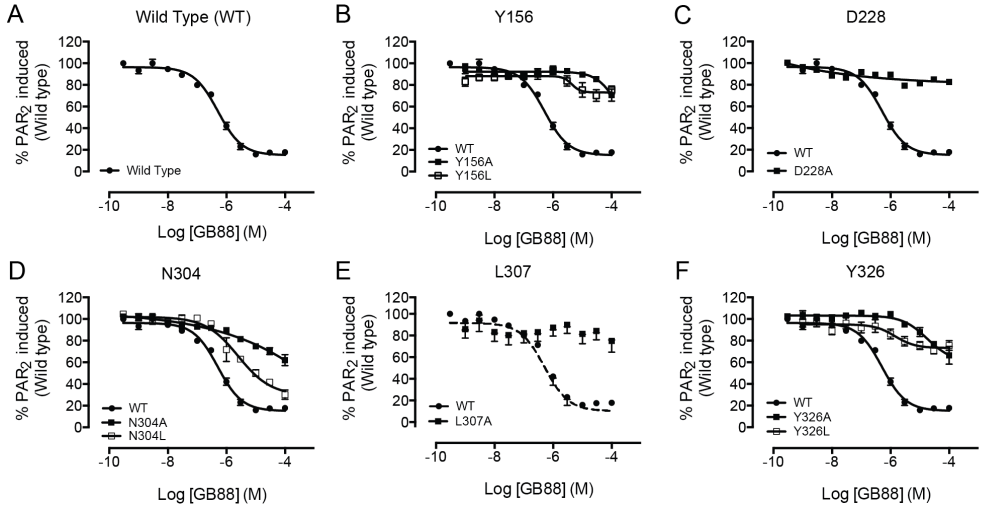

FIGURE 6. Concentration response curves of GB88 antagonism on various PAR_2 mutants. Dose response curves of GB88 inhibition against trypsin (EC_{80}) on various

496 mutants (A, Wild type; B, Y156; C, D228; D, N304; E, L307; F, Y326). Data points =

497 means of 3 experiments in triplicates (n=3), bars = S.E.

498

Table 2. PAR_2 mutants reducing GB88 antagonism of trypsin-induced iCa^{2+} release in CHO-$hPAR_2$ cells

	Max. inhibition (% ± SEM)	GB88 (n ≥ 3)			EC_{80} Trypsin (nM)
		pIC_{50} ± SEM	IC_{50} (uM)	Fold	
Wild Type	80 ± 2	6.3 ± 0.1	0.5	1	20
Y82A*	n.d.	n.d.	n.d.	n.d.	-
F128A	80 ± 4	6.0 ± 0.2	1	2	45
F128L	70 ± 2	5.5 ± 0.2	3	6	30
L151A	65 ± 3	5.7 ± 0.1	22	44	30
F155A	70 ± 5	6.0 ± 0.1	1	2	30
F155L	60 ± 2	5.6 ± 0.3	2	4	230
Y156A	30 ± 5	inactive	-	-	70
Y156L	25 ± 4	inactive	-	-	70
Y160L	70 ± 5	6.3 ± 0.3	0.5	1	60
D228A	20 ± 2	inactive	-	-	130
E322A	70 ± 3	5.8 ± 0.1	1.5	3	80
Q233A	80 ± 2	6.3 ± 0.1	0.5	1	50
E322AQ233A	80 ± 4	6.3 ± 0.1	0.5	1	30
F243A	60 ± 3	5.2 ± 1.2	7	14	60
L246A	80 ± 4	6.5 ± 0.2	0.3	0.6	240
V250A	90 ± 4	7.0 ± 0.1	0.9	1.8	40
F251A	60 ± 6	5.7 ± 0.5	2	4	70
Y296A	90 ± 1	6.5 ± 0.1	0.3	0.6	90
S303A	80 ± 2	6.0 ± 0.1	1	2	25
N304A	40 ± 5	inactive	-	-	230
N304L	70 ± 4	5.6 ± 0.3	3	6	230
L307A	25 ± 6	inactive	-	-	30
V308A	80 ± 3	6.2 ± 0.2	0.7	1.4	20
Y311A	90 ± 2	6.8 ± 0.1	0.2	0.4	110
Y311L	70 ± 5	7.5 ± 0.2	0.03	0.06	40
Y326A	30 ± 8	inactive	-	-	60
Y326L	25 ± 4	inactive	-	-	40
L330W	95 ± 1	6.4 ± 0.1	0.4	0.8	30

n = number of independent experiment, % ± Standard Error of Mean
Fold Change = IC_{50} mutant / IC_{50} Wild Type
*GB88 was not tested in Y82A due to small agonist response
inactive – GB88 failed to inhibit >40% of agonist response
EC_{80} Trypsin – Trypsin concentration used to induce PAR_2 activation
pIC_{50} = -logIC_{50}

GB88 antagonism of 2f-LIGRLO-NH2 and GB110 induced activation of PAR_2

Analysis of the effect of increasing concentrations of GB88 on Ca^{2+} release, induced by escalating doses of 2f-LIGRLO-NH_2 and GB110, revealed that on CHO-hPAR_2WT, GB88 caused a rightward horizontal shift of agonist concentration-response curves (Fig. 7A,B) and by Schild plots, which had linear slopes of 0.95 ± 0.1 and 1.15 ± 0.14 respectively (Fig. 7C,D). Slight reductions of the maxima were also observed. It could be caused by the short assay timeframe, preventing the system to reach true equilibrium and leads to subsequent depression of maxima. Incubation time was reduced in order to investigate potential kinetic artifact (Charlton and Vauquelin 2010; Kenakin et al., 2006), however, GB88 was inactive against both 2f-LIGRLO-NH_2 and GB110 in the iCa^{2+} assay without pre-incubation (Fig. 8A,B). Furthermore, reduction of incubation time from 30 min to 5 min failed to recover the maxima (Fig. 8C,D).

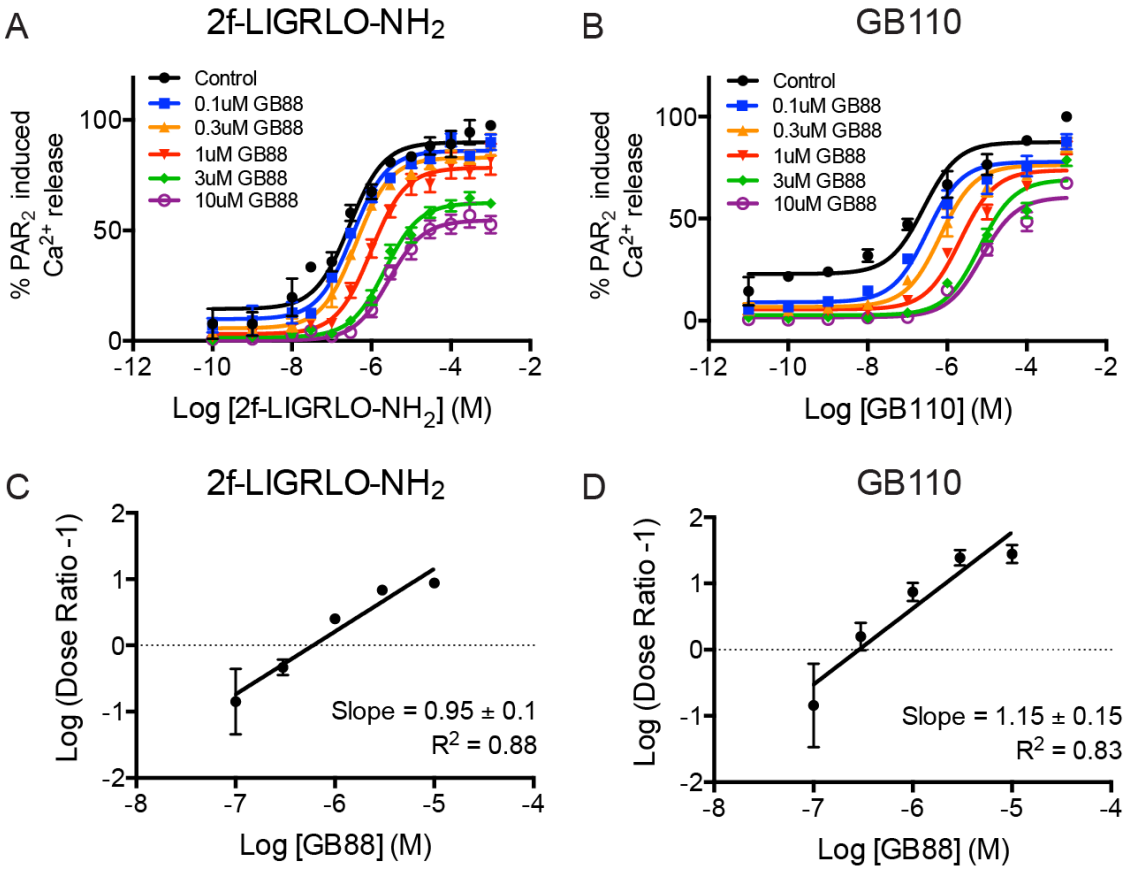

512

513 **FIGURE 7.** Antagonism of GB88 in CHO-hPAR$_2$ wild type. (A-B) GB88 is a competitive
514 PAR$_2$ antagonist against (A) 2f-LIGRLO-NH$_2$ and (B) GB110. (C-D) Schild plot for
515 antagonist GB88 against (C) 2f-LIGRLO-NH$_2$ and (D) GB110. Calculated pA$_2$ values for
516 GB88 against 2f-LIGRLO-NH$_2$ and GB110 was 6.2 ± 0.2 and 6.5 ± 0.2 respectively. Data
517 points = means of 3 experiments in triplicates (n=3), bars = S.E.

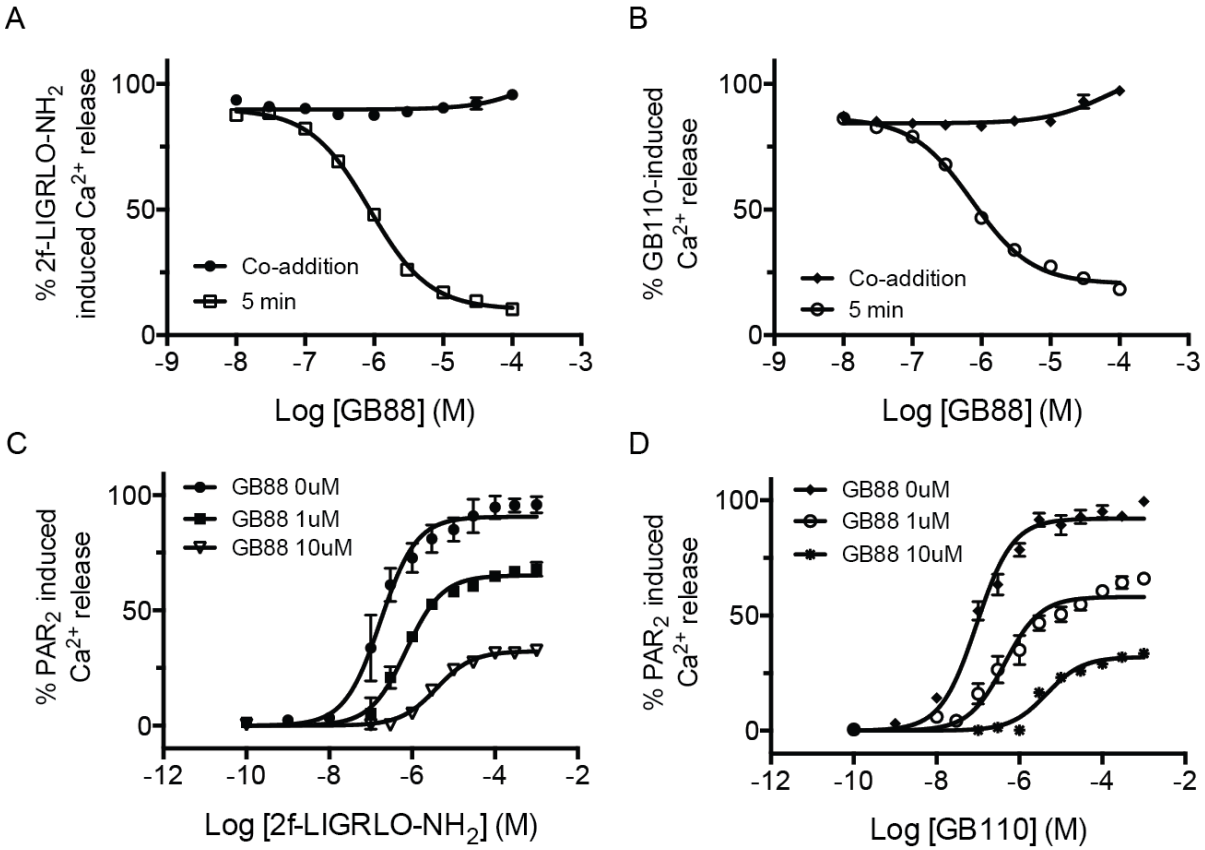

FIGURE 8. Kinetic study of GB88 antagonism of PAR_2 in CHO-hPAR_2 wild type. (A-B) Increasing concentrations of GB88 were added either 5 min prior to agonist addition or simultaneously with agonist and measured for intracellular calcium release. GB88 was only able to inhibit (A) 2f-LIGRLO-NH_2 (10 μM) or (B) GB110 (10 μM) after 5 min pre-incubation. (C-D) Reduction in pre-incubation time failed to reduce maxima reduction. Pre-incubation time of GB88 was shortened from our normal exposure of 30 min to just 5 min prior to agonist addition. No significant changes in maxima reduction as a result of shorter antagonist incubation time. Data points are means of at least 3 experiments in triplicate ($n \geq 3$), bars = S.E.

As mentioned earlier, most of the mutations caused a similar potency reduction for each of the two synthetic agonists, with the exception of F155A, V250A and L307A. These three mutants reduced GB110 potency to a much greater extent (10-, 17- and 54-fold respectively) than did 2f-LIGRLO-NH_2 (3-, 2- and 4-fold respectively). These differences in potency

533 reductions suggested subtly different interactions between the two synthetic ligands and
534 PAR_2, so we similarly inspected corresponding effects on the antagonist GB88. As L307A
535 was ruled out due to its inactivation of the antagonist (Table 2, max inhibition 25%), further
536 experiments were performed on the remaining two mutants (F155A, V250A). When IC_{50}
537 values of GB88 were calculated by increasing its concentration against a fixed agonist
538 concentration, no significant difference was observed against each of the 2 agonists in each of
539 the 3 cell lines (WT, F155A, V250A) (Fig. 9A, B). However, as shown in Fig. 10 this was
540 not true when a Schild plot analysis was performed. F155A showed similar results as wild
541 type-PAR_2 for antagonism by GB88 against the two synthetic agonists, i.e. increasing
542 concentrations of GB88 resulted in horizontal shifts in concentration-response curves of both
543 2f-LIGRLO-NH_2 (Fig. 9C) and GB110 (Fig. 9D). In contrast to WT and F155A, V250A
544 showed distinct differences in affecting each synthetic agonist. When GB88 was used to
545 inhibit 2f-LIGRLO-NH_2, reduction of maxima was significantly greater at >1 μM (Fig. 9E),
546 whereas a similar maxima reduction was not observed when GB110 was used as agonist (Fig.
547 9F). This indicated that the V250A mutation turned GB88 into an insurmountable antagonist
548 against 2f-LIGRLO-NH_2, but not against GB110.
549

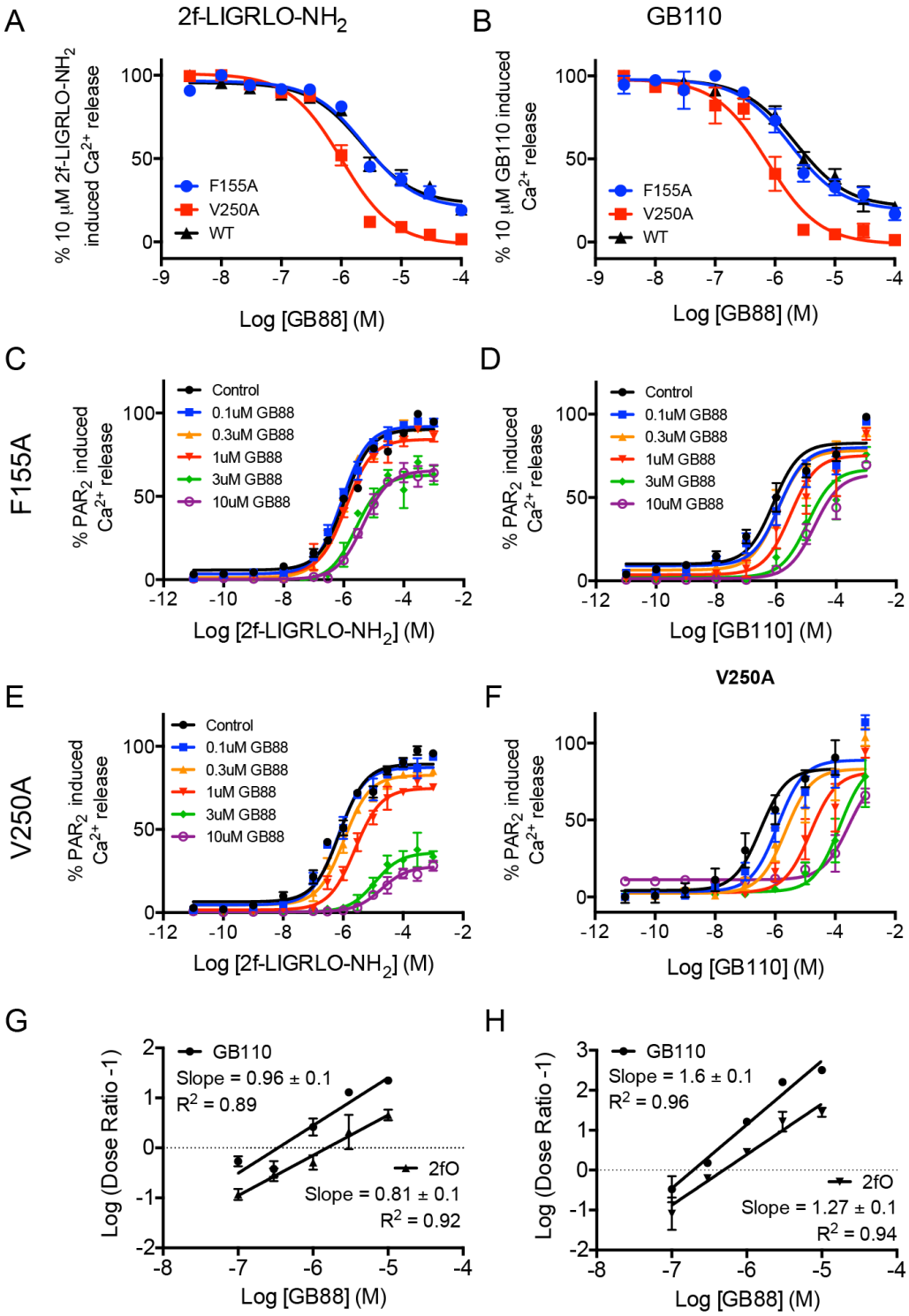

FIGURE 9. Antagonism of GB88 in mutants. (A,B) PAR_2 antagonist GB88 inhibits iCa^{2+} release induced in CHO transfected with wild type PAR_2 or mutants (F155A, V250A) by (A) 2f-LIGRLO-NH_2, or (B) GB110. (A) GB88 IC_{50}s against 2f-LIGRLO-NH_2 are WT, 2 μM ± 0.4 μM; F155A, 2.4 μM ± 0.6 μM; V250A, 1 μM ± 0.3 μM. (B) GB88 IC_{50}s against 2f-LIGRLO-NH_2 are WT, 2.2 μM ± 0.6 μM; F155A, 1.8 μM ± 0.6 μM; V250A, 0.8 μM ± 0.3

556 μM. (C,D) GB88 is a competitive PAR_2 antagonist against (C) 2f-LIGRLO-NH_2 and (D)
557 GB110 in F155A. (E,F) GB88 is an insurmountable antagonist against (E) 2f-LIGRLO-NH_2
558 but a surmountable antagonist against (F) GB110 in V250A. (G,H) Schild plot for antagonist
559 GB88 against 2f-LIGRLO-NH_2 and GB110 in F155A and V250A. (G) Calculated pA_2 values
560 for GB88 against 2f-LIGRLO-NH_2 and GB110 in F155A was 5.8 ± 0.15 and 6.5 ± 0.2,
561 respectively. (H) Calculated pA_2 values for GB88 against 2f-LIGRLO-NH_2 and GB110 in
562 V250A was 6.3 ± 0.15 and 6.7 ± 0.1 respectively Data points = means of 3 experiments in
563 triplicates (n=3), bars = S.E.
564
565 Schild slope analysis further validated the differences between F155A and V250A.
566 F155A produced a linear gradient of 0.81 ± 0.1 for 2f-LIGRLO-NH_2 and 0.96 ± 0.1 for
567 GB110, indicating GB88 is a competitive antagonist against both synthetic agonists in F155A
568 PAR_2 (Fig. 9G). In comparison, V250A produced steeper Schild slopes of 1.3 ± 0.1 (2f-
569 LIGRLO-NH_2) and 1.6 ± 0.1 (GB110) (Fig. 9H). A Schild slope >1 can indicate insufficient
570 equilibration time, and GB88 may not have attained equilibrium at lower concentrations, thus
571 changing the gradient of the Schild plot. A steep slope can also imply binding cooperativity
572 of an antagonist, where the V250A mutation enables binding of more than one molecule of
573 GB88. In either case, V250A mutation significantly changed how the receptor interacts with
574 the agonist/antagonist. F155A also reduced the pA_2 of GB88 against 2f-LIGRLO-NH_2 from
575 6.2 (wild type) to 5.8, but the pA_2 value of GB88 against GB110 remained unchanged at 6.5,
576 while V250A had no significant changes in pA_2 of GB88 against both agonists.
577
578

Discussion and Conclusions

This is the first detailed analysis of the importance of amino acids in the transmembrane region of PAR_2 for dictating intracellular Ca^{2+} release induced by PAR_2 ligands. This study monitored effects of PAR_2 mutations on calcium release, a signaling pathway commonly used for PAR_2 research and previously shown to dictate inflammatory responses of PAR_2 agonists 2f-LIGRLO-NH_2, GB110, trypsin and the pathway selective anti-inflammatory antagonist GB88, both *in vitro* and *in vivo* in rodents (Suen et al, 2012; Suen et al 2014; Lohman et al, 2012a). This approach was used rather than a competitive binding assay for comparative ligand affinities for PAR_2 because, unlike other GPCRs, there is no orthosteric ligand for PAR_2 that can be used exogenously to compete with, since only proteases are known to endogenously activate PAR_2. Thus, in order to correlate receptor binding with receptor activity, we instead performed a receptor saturation assay using 2f-LIGRLO(dtpa)-NH_2 on PAR_2. Ten cell lines (WT, Vector, 8 mutants) were found to change the observed K_d values of this exogenous in a similar manner in the receptor saturation assay as in the calcium assay, strongly supporting the validity of using the calcium functional assay for measuring receptor mutant effects on ligand binding.

This study has identified for the first time that the transmembrane region of PAR_2 is crucial for receptor activation by the synthetic ligands described herein, as defined by ligand binding and by induction of intracellular calcium signaling (Fig. 10). in particular, four transmembrane mutations (Y82A, Y296A, N304A and N304L) reduced potencies of all three agonists examined here and highlighted the importance of those residues in PAR_2 activation. Furthermore, we examined 28 mutations of PAR_2 and found a cluster of residues defining a 'hot spot' within the TM region of the receptor that is critical for PAR_2-mediated signal transduction by these ligands, potentially due to changes in ligand-receptor interactions. Eight TM mutants (Y82, F155, Y156, F251, Y296, N304, Y311 and Y326) affected both of the two

synthetic agonists similarly. Three of these residues (Y82, Y156 and Y326), along with ECL2 residue D228, were the most important for PAR_2 activation (> 100 fold) induced by GB110 and 2f-LIGRLO-NH_2. It is interesting to note that these two synthetic agonists did not give entirely identical responses, with two mutations (V250 and L307) showing significant differences between the effects of these agonists.

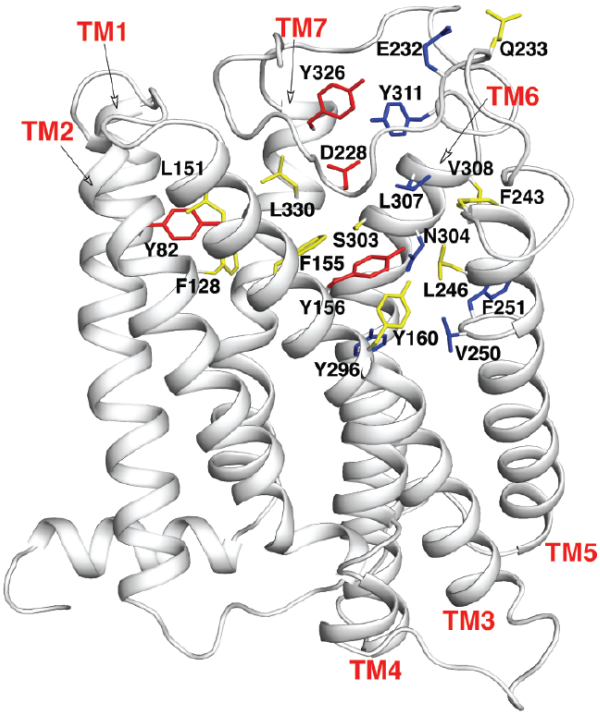

FIGURE 10. Summary of PAR_2 mutations that impact synthetic ligand-induced signaling. All residues selected for mutagenesis in this study are highlighted in the PAR_2 model. Residues found to affect agonist activity (Table 1) are colored in red (>100 fold), blue (>15 fold) and yellow (<15 fold).

This is the first time that PAR_2 has been mutated at multiple positions within and around its transmembrane region. There have only been a few previous reports (Compton et al., 2000; Compton et al., 2002; Ma et al., 2013) of PAR_2 mutations at all and they focused only on one or a few mutations in ECL2 but not in the TM region. The findings here of the importance of TM region to ligand-induced activation as measured by Ca^{2+} release are novel

620 and demonstrate a significant role of the TM region in PAR_2 activation and downstream
621 signal transduction. This study has also established that PAR_2 signaling is similar to other
622 class A GPCRs, where the TM region has been shown to be crucial for interaction with
623 agonists and antagonists (Tyndall et al., 2005; Blakeney et al., 2007; Ruiz-Gómez et al.,
624 2010) with strong support from crystal structures and computer models (Deupi and Standfuss,
625 2011; Nakamura et al., 2013).

626 The original ligand binding predictions were derived from a PAR_2 homology model
627 built from rhodopsin some years ago when this was the only class A GPCR with a reported
628 crystal structure. Following the completion of this study, new crystal structures have become
629 available for class A GPCRs, including ORL-1 (PDB: 4EA3) (Thompson et al., 2012) and
630 PAR_1 (PDB: 3VW7) (Zhang et al., 2012). The ligands described herein were re-docked into
631 new homology models built (Perry et al., 2015) from these crystal structures. The PAR_1-
632 derived PAR_2 model was problematic (despite high sequence similarity) because the bound
633 ligand vorapaxar was large and believed to distort the structure of PAR_1. Vorapaxar does not
634 bind to PAR_2, so the high sequence identity of PAR_1 and PAR_2 created a problem with an
635 unusual ligand-binding site being created for PAR_2. Nonetheless, the predictions of the
636 binding modes in both of these two additional models encouragingly overlapped with 40% of
637 the residues predicted from the rhodopsin-based model, including almost all of the key
638 residues.

639 There have been concerns that rhodopsin as a modelling basis may unfairly bias
640 toward an internal TM binding site, as the rhodopsin receptor itself has a covalently bound
641 internal ligand. Although it is possible that the docking results from our model have been
642 influenced by this, recent class A GPCRs have also been shown to share a common TM
643 binding location as to that in rhodopsin (Congreve et al., 2011), suggesting an internal
644 binding pocket is not unique to rhodopsin, but common among class A GPCRs. This was

evidenced further by a recent crystal structure of CCR5 bound to its allosteric inhibitor maraviroc (Tan et al., 2013). Furthermore, the rhodopsin template has been successfully used for homology modelling of other GPCRs, such as leukotriene receptor (Dong et al., 2013), alpha1A receptor (Evers and Klabunde 2005), beta2 adrenoceptor (Costanzi 2008), MT1 and MT2 receptors (Farce et al., 2008). It is important to note that there are limitations with homology structures derived from low sequence homology, which has encouraged the development of GPCR models from different crystal structures. It has been reported that there is no correlation between sequence identity and model quality (Ratai et al, 2014), and our use of three PAR2 homology models derived from three different GPCR crystal structures does highlight a conserved subset of PAR2 residues that warranted mutation.

Our data has shown that PAR_2 activation by two synthetic agonists (2f-LIGRLO-NH_2, GB110) was mainly affected by PAR_2 mutations clustered within the TM region, whereas receptor activation by trypsin was largely unaffected by these mutations. Most mutations on GPCRs alter ligand activity either (i) directly by altering the specific binding site of the ligand or (ii) indirectly by changing receptor conformation with a knock-on or induced fit influence on ligand-receptor interaction. While results of this study alone cannot precisely unravel the mechanisms of PAR_2 activation, it is clear that the synthetic agonists examined were significantly more susceptible than trypsin to these changes in the TM region of PAR_2. In our opinion, the finding that over 20 amino acids clustered in the TM region of PAR_2 strongly influence the actions of three synthetic ligands, but not the trypsin-induced native ligand, is suggestive of different ligand-binding sites on PAR_2. While this 'hot spot' within PAR_2 is possibly an allosteric, rather than orthosteric, ligand-binding site, further studies and indeed PAR_2 crystal structures are required to confirm this hypothesis.

This study has involved a diverse set of PAR_2 mutations to probe the differential effects of a narrow group of synthetic ligands on PAR_2-induced calcium release and identifies

a receptor 'hot spot' within the TM region of the receptor that is critical for PAR_2-mediated calcium release by these ligands. Further sets of mutants in the ECL regions and the TM-solvent interface could similarly be used to identify residues important for different tethered ligands, known to be exposed by the actions of different endogenous proteases (e.g. trypsin, tryptase, factor VIIa, cathepsin S, elastase, etc). There have been a few other small molecule agonists (e.g. AC-55541, AC-264613 (Seitzberg et al., 2008)) and antagonists (e.g. ENMD-1068 (Kelso et al., 2006), K14585 (Kanke et al., 2009; McIntosh et al., 2010), C391 (Boitano et al., 2015)) reported to modulate PAR_2 in recent years, as well as many proteases and peptides (Hollenberg et al., 2014; Zhao et al., 2014b), including some peptides with lipid appendages (e.g. P2pal-18S (Sevigny et al., 2011), 2at-LIGRL-PEG_3-hdc (Flynn et al., 2013)). It is not known where any of these compounds bind on PAR_2 and so studies like that reported here could reveal similar or new receptor 'hot spots' required for ligand-induced PAR_2 signaling.

An additional level of complexity lies in a downstream signaling pathway being monitored for such studies. Recent identification of biased ligands for PAR_2 (Ramachandran et al., 2014; Suen et al., 2014; Zhao et al., 2014b) suggests that different signaling pathways may be subtly influenced by only small changes to ligands, which in turn alter interactions with the receptor. Other studies have shown that mutations in the tethered ligand region of PAR_2 can differentially activate different signaling pathways (e.g. Ca^{2+}, MAPK) (Ramachandran et al., 2009; Elmariah et al., 2014), different proteases can induce different signaling profiles (Elmariah et al., 2014; Zhao et al., 2014a; Zhao et al., 2014b), different small molecule ligands can bias signaling to different outcomes (Goh et al., 2009; Hollenberg et al., 2014), and different cell types and reporter assays can produce different PAR_2 signaling. Linking these effects to specific residues in the receptor and specific components of the ligand, as we have begun to do in this study, can dramatically help improve our

695 understanding of the molecular basis of PAR_2-directed intracellular signaling and may permit
696 development of drugs that control different PAR_2-mediated signaling pathways in different
697 physiological and disease settings. This is important because PAR_2 (like other GPCRs) has
698 beneficial and protective physiological effects that may need to be preserved, while
699 selectively modulating just one or a subset of PAR2-mediated signaling pathways associated
700 with a particular diseased state may be more desirable. Studies such as this contribute to our
701 understanding of ligand-induced PAR_2 signaling, while future studies are needed to
702 determine the direct mechanisms employed for activation versus inhibition of different
703 signaling pathways mediated by the same receptor and different (or even the same) ligands.
704

705 **Acknowledgments**

706 We acknowledge financial support from the Australian Research Council (grant
707 DP130100629), ARC Centre of Excellence in Advanced Molecular Imaging (CE140100011),
708 National Health and Medical Research (grants 569595, 614206, 1047759, 1083131) and the
709 Queensland Government for a CIF grant. DPF acknowledges ARC Federation (FF668733)
710 and NHMRC Senior Principal Research (1027369) fellowships, JDH acknowledges an ARC
711 Future Fellowship FT120100917 and MNA acknowledges a NHMRC Early Career
712 Fellowship (1091589). We also thank Professor Christopoulos (Monash University) for a
713 helpful discussion.
714

715 **Conflicts of Interest**

716 JS, JL, MKY and DF are named inventors on several patent applications involving PAR_2
717 agonists and antagonists owned by the University of Queensland. No other competing
718 interests.
719

Author contributions

JS, MNA, WX, JH and DF wrote the manuscript; WX, PKM created the computer models; MNA, YF and YH developed the PAR_2 mutants; JS, MNA, JL and AC performed all of the cell experiments.

REFERENCES

Abey HT, Fairlie DP, Moffatt JD, Balzary RW, Cocks TM (2006) Protease-activated receptor-2 peptides activate neurokinin-1 receptors in the mouse isolated trachea. *J Pharmacol Exp Ther* **317**:598-605

Adams MN, Christensen ME, He Y, Waterhouse NJ, Hooper JD (2011). The role of palmitoylation in signalling, cellular trafficking and plasma membrane localization of protease-activated receptor-2. *PLoS One* **6**:e28018

Adams MN, Pagel CN, Mackie EJ, Hooper JD (2012). Evaluation of antibodies directed against human protease-activated receptor-2. *N-S Arch Pharmacol* **385**:861-873

Adams MN, Ramachandran R, Yau MK, Suen JY, Fairlie DP, Hollenberg MD, *et al.* (2011). Structure, function and pathophysiology of protease activated receptors. *Pharmacol Ther* **130**:248-282

Al-Ani B, Saifeddine M, Kawabata A, Hollenberg MD (1999). Proteinase activated receptor 2: Role of extracellular loop 2 for ligand-mediated activation. *Br J Pharmacol* **128**:1105-1113

Alexander SPH, Benson HE, Faccenda E, Pawson AJ, Sharman JL, McGrath JC, *et al*. (2013). The concise guide to pharmacology 2013/14. *Br J Pharmacol* **170**:1449-1458

Badeanlou L, Furlan-Freguia C, Yang G, Ruf W, Samad F (2011). Tissue factor-protease-activated receptor 2 signaling promotes diet-induced obesity and adipose inflammation. *Nat Med* **17**:1490-1497

747 Ballesteros JA, Weinstein H (1995). Integrated methods for the construction of three
748 dimensional models and computational probing of structure-function relations
749 in G-protein coupled receptors. *Methods Neurosci* **25**:366-428.
750 Barry GD, Le GT, Fairlie DP (2006). Agonists and antagonists of protease activated
751 receptors (PARs). *Curr Med Chem* **13**:243-265
752 Barry GD, Suen JY, Le GT, Cotterell A, Reid RC, Fairlie DP (2010). Novel agonists
753 and antagonists for human protease activated receptor 2. *J Med Chem*
754 **53**:7428-7440
755 Bissantz C, Bernard P, Hibert M, Rognan D (2003). Protein-based virtual screening of
756 chemical database. II. Are homology models of G-Protein Coupled Receptors
757 suitable targets? *Proteins* **50**:5-25
758 Blakeney JS, Reid RC, Le GT, Fairlie DP (2007). Nonpeptidic Ligands For Peptide-
759 Activated GPCRs. *Chem Rev* **107**:2960-3041.
760 Bohm SK, Kong W, Bromme D, Smeekens SP, Anderson DC, Connolly A, *et al*.
761 (1996). Molecular cloning, expression and potential function of the human
762 proteinase-activated receptor-2. *Biochem J* **314**:1009-1016
763 Boitano S, Hoffman J, Flynn AN, Asiedu MN, Tillu DV, Zhang Z, *et al*. (2015). The
764 novel PAR2 ligand C391 blocks multiple PAR2 signalling pathways in vitro
765 and in vivo. *Br J Pharmacol* **172**:4535-4545
766 Boitano S, Hoffman, J, Tillu DV, Asiedu MN, Zhang Z, Sherwood CL, *et al*. (2014).
767 Development and evaluation of small peptidomimetic ligands to protease-
768 activated receptor-2 (PAR2) through the use of lipid tethering. *PLoS One*
769 **9**:e99140
770 Charlton SJ, Vauquelin G (2010). Elusive equilibrium: the challenge of intrepreting
771 receptor pharmacology using calcium assays. *Br J Pharmacol* **161**:1250-1265

772 Compton SJ, Cairns JA, Palmer KJ, Al-Ani B, Hollenberg MD, Walls AF (2000). A
773 polymorphic Protease-activated Receptor 2 (PAR2) displaying reduced
774 sensitivity to trypsin and differential responses to PAR agonists. *J Biol Chem*
775 **275**:39207-39212
776 Compton SJ, Sandhu S, Wijesuriya SJ, Hollenberg MD (2002). Glycosylation of
777 human proteinase-activated receptor-2 (hPAR2): role in cell surface
778 expression and signalling. *Biochem J* **368**: 495-505
779 Congreve M, Langmead CJ, Mason JS, Marshall FH (2011). Progress in structure
780 based drug design for G protein-coupled receptors. *J Med Chem* **54**:4283-4311
781 Costani S (2008). On the applicability of GPCR homology models to computer-aided
782 drug discovery: a comparison between in silico and crystal structures of the
783 beta2-adrenergic receptor. *J Med Chem* **51**:2907-2914
784 Coughlin SR (2000). Thrombin signalling and protease-activated receptors. *Nature*
785 **407**:258-264
786 Coughlin SR and Camerer E (2003). PARticiplation in inflammation. *J Clin Invest*
787 **111**:25-27
788 Dery O, Corvera CU, Steinhoff M, Bunnett NW (1998). Proteinase-activated
789 receptors: novel mechanisms of signaling by serine proteases. *Am J Physiol*
790 **274**:C1429-1452
791 Deupi X and Standfuss J (2011) Structural insights into agonist-induced activation of
792 G-protein-coupled receptors. *Curr Opin Struct Biol* **21**:541-551
793 Dong X, Zhao Y, Huang X, Lin K, Chen J, Wei E, *et al.* (2013). Structure-based drug
794 design using GPCR homology modeling: toward the discovery of novel
795 selective CysLT2 antagonists. *Eur J Med Chem* **62**:754-763

796 Elmariah SB, Reddy VB, Lerner EA (2014). Cathepsin S signals via PAR2 and
797 generates a novel tethered ligand receptor agonist. *PLoS One* **9**:e99702
798 Evers A (2005). Structure-based drug discovery using GPCR homology modeling:
799 successful virtual screening for antagonists of the alpha1A adrenergic
800 receptor. *J Med Chem* **48**:1088-1097
801 Farce A, Chugunov AO, Loge C, Sabaouni A, Yous S, Dilly S, et al. (2008).
802 Homology modeling of MT1 and MT2 receptors. *Eur J Med Chem* **43**:1926-
803 1944
804 Flynn AN, Hoffman J, Tillu DV, Sherwood CL, Zhang Z, Patek R, *et al*. (2013).
805 Development of highly potent protease-activated receptor 2 agonists via
806 synthetic lipid tethering. *FASEB J* **27**:1498-1510
807 Goh FG, Ng PY, Nilsson M, Kanke T, Plevin R (2009) Dual effect of the novel
808 peptide antagonist K-14585 on proteinase-activated receptor-2-mediated
809 signalling. *Br J Pharmacol* **158**:1695-1704
810 Hoffman J, Flynn AN, Tillu DV, Zhang Z, Patek R, Price TJ*, et al.* (2012).
811 Lanthanide labeling of a potent protease activated receptor-2 agonist for time-
812 resolved fluorescence analysis. *Bioconjugate Chem* **23**:2098-2104
813 Hollenberg MD, Mihara K, Polley D, Suen JY, Han A, Fairlie DP, *et al.* (2014).
814 Biased signalling and proteinase-activated receptors (PARs): targeting
815 inflammatory disease *Br J Pharmacol* **171**:1180-1194
816 Hollenberg MD, Saifeddine M, al-Ani B, Kawabata A (1997). Proteinase-activated
817 receptors: structural requirements for activity, receptor cross-reactivity, and
818 receptor selectivity of receptor-activating peptides. *Can J Physiol Pharmacol*
819 **75**:832-841

820 Jones G, Willett P, Glen RC, Leach AR, Taylor R (1997). Development and
821 validation of a genetic algorithm for flexible docking. *J Mol Biol* **267**:727-748
822 Kanke T, Ishiwata H, Kabeya M, Saka M, Doli T, Hattori Y, *et al.* (2005). Binding of
823 a highly potent protease-activated receptor-2 (PAR2) activating peptide,
824 [^{3}H]2-furoyl-LIGRL-NH_2, to human PAR2. *Br J Pharmacol* **145**:255-263
825 Kanke T, Kabeya M, Kubo S, Kondo S, Yasuoka K, Tagashira J, *et al.* (2009) Novel
826 antagonists for proteinase-activated receptor 2: inhibition of cellular and
827 vascular responses in vitro and in vivo. *Br J Pharmacol* **158**:361-371
828 Kelso EB, Lockhart JC, Hembrough T, Dunning L, Plevin R, Hollenberg MD, *et al.*
829 (2006) Therapeutic promise of proteinase-activated receptor-2 antagonism in
830 joint inflammation. *J Pharmacol Exp Ther* **316**:1017-1024
831 Kenakin T, Jenkinson S, Watson C (2006). Determining the potency and molecular
832 mechanism of action of insurmountable antagonists. *J Pharmacol Exp Ther*
833 **319**:710-723
834 Lim J, Iyer A, Liu L, Suen JY, Lohman RJ, Seow V, *et al.* (2013). Diet-induced
835 obesity, adipose inflammation, and metabolic dysfunction correlating with
836 PAR2 expression are attenuated by PAR2 antagonism. *FASEB J* **27**:4757-
837 4767
838 Lin C, Von Der Thusen J, Daalhuisen J, Ten Brink M, Crestani B, Van Der Poll T, *et*
839 *al.* (2015) Pharmacological targeting of protease activated receptor-2 affords
840 protection from bleomycin-induced pulmonary fibrosis. *Mol Med* Epub
841 doi:10.2119/molmed.2015.00094
842 Lohman RJ, Cotterell AJ, Barry GD, Liu L, Suen JY, Vesey DA, *et al.* (2012a). An
843 antagonist of human protease activated receptor-2 attenuates PAR2 signaling,

macrophage activation, mast cell degranulation, and collagen-induced arthritis in rats. *FASEB J* **26**:2877-2887

Lohman RJ, Cotterell AJ, Suen J, Liu L, Do AT, Vesey DA, *et al.* (2012b). Antagonism of protease-activated receptor 2 protects against experimental colitis. *J Pharmacol Exp Ther* **340**:256-265

Lovell SC, Word JM, Richardson JS, Richardson DC (2000). The penultimate rotamer library. *Proteins* **40**:389-408

Ma JN, Burstein ES (2013). The PAR2 polymorphic variant F240S constitutively activates PAR2 receptors and potentiates responses to small molecule PAR2 agonists. *J Pharmacol Exp Ther* **374**:697-704

Maryanoff BE, Santulli RJ, McComsey DF, Hoekstra WJ, Hoey K, Smith CE, *et al.* (2001). Protease-Activated Receptor-2 (PAR-2): Structure-Function study of receptor activation by diverse peptides related to tethered-ligand epitopes. *Arch Biochem Biophys* **386**:195-204

McGuire JJ, Saifeddine M, Triggle CR, Sun K, Hollenberg MD (2004). 2-furoyl-LIGRLO-amide: a potent and selective proteinase-activated receptor 2 agonist. *J Pharmacol Exp Ther* **309**:1124-1131

McIntosh K, Cunningham MR, Cadalbert L, Lockhart J, Boyd G, Ferrell WR, *et al.* (2010) Proteinase-activated receptor-2 mediated inhibition of TNFalpha-stimulated JNK activation – A novel paradigm for G(q/11) linked GPCRs. *Cell Signal* **22**:265-273

Nakamura S, Itabashi T, Ogawa D, Okada T (2013). Common and distinct mechanisms of activation of rhodopsin and other G protein-coupled receptors. *Sci Rep* **3**:1844

868 Palczewski K, Kumasaka T, Hori T, Behnke CA, Motoshima H, Fox BA, *et al.*
869 (2000). Cyrstal structure of rhodopsin: A G protein-coupled receptor. *Science*
870 **289**:739-745
871 Ramachandran R, Mihara K, Chung H, Renaux B, Lau CS, Muruve DA, *et al.* (2011).
872 Neutrophil elastase acts as a biased agonist for proteinase-activaetd receptor-2
873 (PAR2). *J Biol Chem* **286**:24638-24648
874 Ramachandran R, Mihara K, Mathur M, Rochdi MD, Bouvier M, Defea K, *et al*.
875 (2009). Agonist-biased signaling via proteinase activated receptor-2:
876 differential activation of calcium and mitogen-activated protein kinase
877 pathways. *Mol Pharmacol* **75**:791-801
878 Ramachandran R, Noorbakhsh F, Defea K, Hollenberg MD. (2012). Targeting
879 proteinase-activated receptors: therapeutic potential and challenges. *Nat Rev*
880 *Drug Discov* **11**:69-86
881 Rataj K, Witek J, Mordalski S, Bojarski AJ. (2014) Impact of template choice on
882 homology model efficiency in virtual screening. *J Chem Inf Model* **54**:1661-
883 1668
884 Ruiz-Gómez G, Tyndall JD, Pfeiffer B, Abbenante G, Fairlie DP (2010). Update 1 of:
885 Over One Hundred Peptide-Activated G Protein-Coupled Receptors
886 Recognize Ligands with Turn Structure. *Chem Rev* **110:**PR1-PR41
887 Sali A and Blundell TL. (1993) Comparative Protein Modelling by Satisfaction of
888 Spatial Restraints. *J Mol Biol* **234**:779-815
889 Seitzberg JG, Knapp AE, Lund BW, Mandrup Bertozzi S, Currier EA, Ma JN, *et al.*
890 (2008) Discovery of potent and selective small-molecule PAR2-agonists. *J*
891 *Med Chem* **51**:5490-5493

892 Sevigny LM, Zhang P, Bohm A, Lazarides K, Perides G, Covic L, *et al.* (2011).
893 Interdicting protease-activated receptor-2 driven inflammation with cell-
894 penetrating pepducins. *PNAS USA* **108**:8491-8496
895 Shi K, Queiroz KC, Stap J, Richel DJ, Spek CA (2013). Protease-activated receptor-2
896 induces migration of pancreatic cancer cells in an extracellular ATP-
897 dependent manner. *J Thromb Haemost* **11:**1892-1902
898 Suen JY, Barry GD, Lohman RJ, Halili MA, Cotterell AJ, Le GT, *et al.* (2012).
899 Modulating human proteinase activated receptor 2 with a novel antagonist
900 (GB88) and agonist (GB110). *Br J Pharmacol* **165**:1413-1423
901 Suen JY, Cotterell A, Lohman RJ, Han A, Yau MK, Liu L, *et al.* (2014). Pathway
902 Selective Antagonism Of Proteinase Activated Receptor 2. *Br J Pharmacol*
903 **171**:4112-4124
904 Tan Q, Zhu Y, Li J, Chen Z, Han GW, Kufareva I, *et al.* (2013). Structure of the
905 CCR5 chemokine receptor-HIV entry inhibitor maraviroc complex. *Science*
906 **341**:1387-1390
907 Thompson AA, Liu W, Chun E, Katritch V, Wu H, Vardy E, *et al.* (2012). Structure
908 of the nociceptin/orphanin FQ receptor in complex with a peptide mimetic.
909 *Nature* **485**:395-399
910 Tyndall JD, Pfeiffer B, Abbenante G, Fairlie DP. (2005). Over 100 Peptide-Activated
911 G Protein-Coupled Receptors Recognize Ligands with Turn Structure. *Chem*
912 *Rev* **105**:793-826.
913 Vesey DA, Suen JY, Seow V, Lohman RJ, Liu L, Gobe GC, *et al.* (2013). PAR2-
914 induced inflammatory responses in human kidney tubular epithelial cells. *Am*
915 *J Physiol Renal Physiol* **304**:F737-750

916 Warne A, Moukhametzianov R, Baker JG, Nehme R, Edwards PC, Leslie AGW, *et*
917 *al.* (2011). The structural basis for agonist and partial agonist action on a b(1)-
918 adrenergic receptor. *Nature* **469**:241-244
919 Waterhouse AM, Procter JB, Martin DM, Clamp M, Barton GJ. (2009). Jalview
920 version 2 – a multiple sequence alignment editor and analysis workbench.
921 *Bioinformatics* **25**:1189-1191
922 Xu F, Wu H, Katritch V, Han GW, Jacobson KA, Gao ZG, *et al.* (2011). Structure of
923 an agonist-bound human A2A adenosine receptor. *Science* **332**:322-327
924 Yau MK, Liu L, Fairlie DP (2013). Towards drugs for protease-activated receptor 2
925 (PAR2). *J Med Chem* **56**:7477–7497
926 Zhang C, Srinivasan Y, Arlow DH, Fung JJ, Palmer D, Zheng Y, *et al*. (2012). High-
927 resolution crystal structure of human protease-activated receptor 1. *Nature*
928 **492**:387-392
929 Zhang J, Zhang K, Gao ZG, Paoletta S, Zhang D, Han GW, et al. (2014). Agonist-
930 bound structure of the human P2Y12 receptor. *Nature* **509**:119-122
931 Zhao P, Lieu T, Barlow N, Metcalf M, Veldhuis NA, Jensen DD, et al. (2014a).
932 Cathepsin S causes inflammatory pain via biased agonism of PAR2 and
933 TRPV4. *J Biol Chem* **289**:27215-21234
934 Zhao P, Metcalf M, Bunnett NW (2014b). Biased signaling of protease-activated
935 receptors. *Front Endocrinol* **5**:67